

Parameter and State Estimation of Vibrating Structures Equipped with Geometrically Consistent Tuned Mass Damper

*A Thesis Phase-II Evaluation Report Submitted
in Partial Fulfillment of the Requirements
for the Degree of*

Bachelor of Technology

by

**Roshan Kumar
(200104093)**

under the guidance of

Dr. Budhaditya Hazra



**to the
DEPARTMENT OF CIVIL ENGINEERING
INDIAN INSTITUTE OF TECHNOLOGY GUWAHATI
GUWAHATI - 781039, ASSAM**

CERTIFICATE

*This is to certify that the work contained in this thesis entitled “**Parameter and State Estimation of Vibrating Structures Equipped with Geometrically Consistent Tuned Mass Damper**” is a bonafide work of **Roshan Kumar** (Roll No. 200104093), carried out in the Department of Civil Engineering, Indian Institute of Technology Guwahati under my supervision and that it has not been submitted elsewhere for a degree.*

Supervisor: **Dr. Budhaditya Hazra**

Associate Professor,
May, 2024
Guwahati. Department of Civil Engineering,
Indian Institute of Technology Guwahati, Assam.

Acknowledgements

I would like to express my sincere gratitude towards my supervisor, Dr. Budhaditya Hazra, for allowing me to work on this wonderful and intricate problem statement. I want to thank him for providing me with his invaluable guidance and encouragement, guiding me throughout this project. He has been a great mentor, from introducing us to non-linear stochastic systems and Manifolds and Lie Algebra to conducting regular productive discussions about this research work. I will forever be indebted to him for this. He always inspires and motivates me to do research work, which helped me with my thesis. I thank the Department of Civil Engineering, IIT Guwahati, for providing the required facilities to complete my research.

I have experienced many new things from his way of working, which will greatly impact my future work. I want to express my special thanks to my seniors, Mr. Satyam Panda, PhD scholar, IIT Guwahati, and Mr. Rohan Prasad, M.Tech Dept. of Civil Engineering, IIT Guwahati, who were there with me every time to solve my issues and helped me to be calm and mentally stable during my project. I am also thankful to my parents for constantly supporting me. I would also like to thank my little brother for his blind love, which always inspired and kept me motivated. Last, I thank Almighty God, Lord Krishna, for giving me blessings and strength.

Roshan Kumar

Roll Number: **200104093**

Contents

List of Figures	ix
1 Introduction	1
1.1 Motivation of the Study	1
1.2 Introduction to Key Concepts	2
1.3 Data and Methods	3
1.4 Objectives of the Present Study	4
1.5 Organisation of the Thesis	4
2 Background	5
2.1 Deterministic and Stochastic Dynamics	5
2.2 Lagrangian and Hamiltonian Dynamics on \mathbb{R}^n	6
2.3 Manifolds	8
2.3.1 Definition	8
2.3.2 Notations	9
2.4 Lie Groups and Lie Algebras	17
2.4.1 Group Axioms	17
2.4.2 Lie Group	17
2.4.3 Group Actions	18
2.4.4 Lie Algebra	18
2.4.5 Exponential Map and Logarithmic Map	18

2.5	Kalman Filter	21
2.5.1	Mathematical Background: Kalman Filter	21
2.5.2	Unscented Kalman Filter on Euclidean Spaces	23
2.5.3	Unscented Kalman Filter on Riemannian Manifolds	27
2.6	Unscented Kalman Filter on Lie Groups	29
2.7	Summary	30
3	State Estimation on Manifolds	31
3.1	Problem Formulation	31
3.2	Spherical Pendulum	32
3.3	Pendulum Cart System	33
3.4	Duffing Oscillator	36
3.5	Double Pendulum	38
3.5.1	Euler–Lagrange Equations in Terms of (q, \dot{q})	38
3.5.2	Euler–Lagrange Equations in Terms of (q, ω)	39
3.6	Filter Design and Initialization	39
3.7	Filtering	40
3.8	Results	40
3.9	Conclusion	40
4	Case Study	43
4.1	Duffing Oscillator	44
4.1.1	Base Case	44
4.1.2	Plots in XY, YZ and ZX Plane	44
4.1.3	High Noise	45
4.1.4	Plots in XY, YZ and ZX Plane	45
4.1.5	Increased Number of Epochs	46
4.1.6	Plots in XY, YZ and ZX Plane	46

4.1.7	Uncertainty Matrix	47
4.1.8	Plots in XY, YZ and ZX Plane	47
4.2	Spherical Pendulum	48
4.2.1	Base Case	48
4.2.2	Plots in XY, YZ and ZX Plane	48
4.2.3	High Noise Std Deviation	49
4.2.4	Plots in XY, YZ and ZX Plane	49
4.2.5	Low Noise Std Deviation	50
4.2.6	Plots in XY, YZ and ZX Plane	51
4.2.7	Change in Initial Condition ($l = 5$)	51
4.2.8	Plots in XY, YZ and ZX Plane	52
4.3	Double Pendulum	52
4.3.1	Plots in XY, YZ and ZX Plane	52
4.4	Pendulum Cart	53
4.4.1	Plots in XY, YZ and ZX Plane	54
5	Conclusion and Future Work	55
5.1	Development of UKF-M	55
5.2	Advanced State Estimation Techniques	55
5.3	Parameter Estimation on Manifolds	56
5.4	De-tuning Strategies	56
5.5	Adaptive Tuning of TMDs and Developments of Active and Passive Controllers on manifolds	56
5.6	Health Monitoring and Maintenance	57
5.7	Conclusion	57
6	Appendix	59
6.1	Software Used	59

6.2 Appendix	60
------------------------	----

References	61
-------------------	-----------

List of Figures

2.1	Manifolds (a) Hypersphere (b) Torus	9
2.2	Geodesic between two points on Sphere	12
2.3	Parallel transport of a vector in a manifold	15
2.4	Exponential Mapping and Logarithmic Mapping on surface of S^2 manifold	16
2.5	Working of Lie Groups and Lie Algebra	19
2.6	Basic Principle of Kalman Filter	21
3.1	Trajectory of Bob of a Spherical Pendulum	33
3.2	Schematic Representation of Pendulum Cart System	34
3.3	Pendulum Cart Simulation.	36
3.4	Pendulum cart Trajectory.	36
3.5	Duffing Oscillator Trajectory	37
3.6	Double Pendulum Simulation.	40
3.7	Double Pendulum Trajectory.	40
3.8	Position Error vs time for UKF and $3 - \sigma$ UKF for Spherical Pendulum. . .	41
3.9	Comparision of True Path and UKF path as Spherical Pendulum evolves with time.	41
3.10	Position Error vs time for UKF and $3 - \sigma$ UKF for Pendulum-Cart System.	41
3.11	Comparision of True Path and UKF path as Pendulum-Cart evolves with time.	41
3.12	Position Error vs time for UKF and $3 - \sigma$ UKF for Duffing Oscillator. . . .	42

3.13 Comparision of True Path and UKF path as Duffing Oscillator evolves with time	42
3.14 Position Error vs time for UKF and $3 - \sigma$ UKF for Double Pendulum.	42
3.15 Comparision of True Path and UKF path as Double Pendulum evolves with time	42
4.1 Position Error vs time for UKF and $3 - \sigma$ UKF for Duffing Oscillator in base base	44
4.2 Position of the components of Duffing Oscillator as a function of time. and Estimated position from the Unscented Kalman Filter (UKF) in base case	44
4.3 True vs Estimated Position (Base Case) in XY plane	44
4.4 True vs Estimated Position (Base Case) in YZ plane	44
4.5 True vs Estimated Position (Base Case) in ZX plane	44
4.6 Position Error vs time for UKF and $3 - \sigma$ UKF for Duffing Oscillator in high noise case	45
4.7 Position of the components of Duffing Oscillator as a function of time and Estimated position from the Unscented Kalman Filter (UKF) in high noise case	45
4.8 True vs Estimated Position (High Noise Case) in XY plane	45
4.9 True vs Estimated Position (High Noise Case) in YZ plane	45
4.10 True vs Estimated Position (High Noise Case) in ZX plane	45
4.11 Position Error vs time for UKF and $3 - \sigma$ UKF for Duffing Oscillator with increased number of epochs	46
4.12 Position of the components of Duffing Oscillator as a function of time and Estimated position from the Unscented Kalman Filter (UKF) with increased number of epochs	46
4.13 True vs Estimated Position (Increased Number of Epochs Case) in XY plane	46
4.14 True vs Estimated Position (Increased Number of Epochs Case) in YZ plane	46

4.15 True vs Estimated Position (Increased Number of Epochs Case) in ZX plane	46
4.16 Position Error vs time for UKF and $3 - \sigma$ UKF for Duffing Oscillator with uncertainty matrix	47
4.17 Position of the components of Duffing Oscillator as a function of time and Estimated position from the Unscented Kalman Filter (UKF) with uncertainty matrix	47
4.18 True vs Estimated Position (Uncertainty Matrix Case) in XY plane	48
4.19 True vs Estimated Position (Uncertainty Matrix Case) in YZ plane	48
4.20 True vs Estimated Position (Uncertainty Matrix Case) in ZX plane	48
4.21 Position Error vs time for UKF and $3 - \sigma$ UKF for Spherical Pendulum in the base case	48
4.22 Position of the components of Spherical Pendulum as a function of time and Estimated position from the Unscented Kalman Filter (UKF) in the base case	48
4.23 True vs Estimated Position (Base Case) in XY plane	49
4.24 True vs Estimated Position (Base Case) in YZ plane	49
4.25 True vs Estimated Position (Base Case) in ZX plane	49
4.26 Position Error vs time for UKF and $3 - \sigma$ UKF for Spherical Pendulum with high noise	49
4.27 Position of the components of Spherical Pendulum as a function of time and Estimated position from the Unscented Kalman Filter (UKF) with high noise	49
4.28 True vs Estimated Position (High Noise Case) in XY plane	50
4.29 True vs Estimated Position (High Noise Case) in YZ plane	50
4.30 True vs Estimated Position (High Noise Case) in ZX plane	50
4.31 Position Error vs time for UKF and $3 - \sigma$ UKF for Spherical Pendulum with low noise	50
4.32 Position of the components of Spherical Pendulum as a function of time and Estimated position from the Unscented Kalman Filter (UKF) with low noise	50

4.33 True vs Estimated Position (Low Noise Case) in XY plane	51
4.34 True vs Estimated Position (Low Noise Case) in YZ plane	51
4.35 True vs Estimated Position (Low Noise Case) in ZX plane	51
4.36 Position Error vs time for UKF and $3 - \sigma$ UKF for Spherical Pendulum with $l = 5$	51
4.37 Position of the components of Spherical Pendulum as a function of time and Estimated position from the Unscented Kalman Filter (UKF) with $l = 5$. .	51
4.38 True vs Estimated Position ($l = 5$) in XY plane	52
4.39 True vs Estimated Position ($l = 5$) in YZ plane	52
4.40 True vs Estimated Position ($l = 5$) in ZX plane	52
4.41 Position Error vs time for UKF and $3 - \sigma$ UKF for Spherical Pendulum in the base case	52
4.42 Position of the components of Spherical Pendulum as a function of time and Estimated position from the Unscented Kalman Filter (UKF) in the base case	52
4.43 True vs Estimated Position (Base Case) in XY plane	53
4.44 True vs Estimated Position (Base Case) in YZ plane	53
4.45 True vs Estimated Position (Base Case) in ZX plane	53
4.46 Position Error vs time for UKF and $3 - \sigma$ UKF for Spherical Pendulum in the base case	53
4.47 Position of the components of Spherical Pendulum as a function of time and Estimated position from the Unscented Kalman Filter (UKF) in the base case	53
4.48 True vs Estimated Position (Base Case) in XY plane	54
4.49 True vs Estimated Position (Base Case) in YZ plane	54
4.50 True vs Estimated Position (Base Case) in ZX plane	54

List of Symbols & Abbreviations

Symbol	Description
GTMD	Geometrically Consistent Tuned Mass Damper
TMD	Tuned Mass Damper
SO(3)	Special Orthogonal Group in three dimensions
PTMD	Pendulum Tuned Mass Damper
dW_t	White Noise
UKF	Unscented Kalman Filter
ω	Angular velocity vector
I	Moment of inertia matrix
u	Control input
$L(q, \dot{q})$	Lagrangian function
q	Configurations (generalized coordinates) of the system
$T(q, \dot{q})$	Kinetic energy of the system
$V(q)$	Potential energy of the system
M	Manifold
\mathcal{M}	Tangent space to the manifold
$\nabla_v w$	Covariant derivative of a vector field
μ_F	Mean Value of Force

Chapter 1

Introduction

Studying dynamical systems helps us understand various phenomena, including earthquakes and chaotic and stochastic motion of natural systems. While the systems can be modeled using traditional Euclidean spaces, the naturally occurring systems are more complicated and complex to model, with the challenges including formulating complex equations involving vibrations, noise, and evolution on complex geometries. Thus, these systems are solved by incorporating geometry in which the systems evolve and the kinematic constraints. Hence, to make sure a structure is safe, Tuned Mass Dampers (TMDs) and pendulum-tuned Mass Dampers (PTMDs) are used to counter the vibration caused by external forces and mitigate the effect of structural vibrations on the integrity and safety of buildings.

1.1 Motivation of the Study

In structural dynamics, the investigation of vibrating systems helps us to find valuable insights into the structural behavior, state of the system, and its response to external forces. These insights are used for De-tuning Strategies, Adaptive Tuning of TMD, and Health Monitoring and Maintenance.

Traditional State estimation on Euclidean Spaces is less robust and has lower accuracy.

Thus, we aim to refine algorithms and methodologies for state estimation of dynamic systems living on manifolds, such as the Special Orthogonal Group $\text{SO}(3)$ or other Lie groups. By enhancing the accuracy and robustness of state estimation, these techniques can enable more precise control of complex systems. Structural systems also often have parameters that may vary or are uncertain, such as mass distributions, material properties, and damping coefficients. Developing methods to simultaneously estimate the state and parameters of such systems while considering the manifold structure can enhance our ability to model and control them effectively.

The intricacies of these systems necessitate a sophisticated modeling approach, and these techniques can be used to design mainly when dealing with structures equipped with geometrically consistent GTMDs. This thesis ventures into the challenging domain of estimating parameters and states of vibrating structures by applying Kalman Filters as a foundational tool for state estimation of Riemannian manifolds over GTMDs.

1.2 Introduction to Key Concepts

PTMDs have emerged as a prominent solution for mitigating structural vibrations induced primarily by dynamic forces such as wind. These devices have found practical application in various full-scale structures, significantly enhancing their ability to withstand environmental forces. The works of A. J. Roffel and Sriram Narasimhan [1] have addressed the need for comprehensive methodologies to estimate modal parameters while PTMDs are in service. Their paper presents a method for time domain modal parametric identification of natural frequencies, mode shapes, and modal damping ratios of structures equipped with PTMDs. This research acknowledges the crucial role of PTMDs in structural dynamics, emphasizing their adaptive passive nature with mechanisms to adjust auxiliary frequency and damping.

One key observation from the studies of Roffel and Narasimhan [1] is the inherent uncertainty associated with estimating the first modal damping. This uncertainty partly

stems from the frequency-dependent behavior of the dampers. Interestingly, this uncertainty is notably reduced for the second mode, suggesting that the damper exhibits less frequency-dependent behavior at higher frequencies. This insight underscores the complexity of PTMDs and highlights the importance of a precise and robust estimation framework for modal parameters, especially in cases involving varying dynamic conditions.

Parallel to the advancements in structural dynamics, differential geometry has gained attention in modeling non-linearities by confining parts of the model to Riemannian manifolds. The work of Søren Hauberg, François Lauze, and Kim Steenstrup Pedersen[2] introduces a novel algorithm that generalizes the unscented transform and the unscented Kalman filter for Riemannian manifolds. This pioneering research provides a generic optimization framework for these domains and demonstrates its robustness and convergence across various applications. In particular, the Riemannian unscented Kalman filter (UKF) is noted for producing smoother motion estimates, making it a promising tool for modeling complex structural vibrations with improved accuracy.

Building on this, the paper by Tripura, Panda, and Hazra [3] extends the horizon of real-time modal identification techniques. Their work introduces a novel approach that leverages first-order error-adapted eigen-perturbation to enhance the accuracy and efficiency of real-time modal identification in vibrating structures. By incorporating differential geometry concepts from Pennec [4] into the identification process, this research represents an innovative step toward addressing the challenges posed by dynamic structural behavior.

1.3 Data and Methods

In this section, we outline the data generation process for simulating structural vibrations equipped with geometrically consistent tuned mass dampers (TMDs) over a manifold using the Geometric Ito-Taylor 1.5 method introduced by Panda and Hazra [5]. Additionally, we provide the dynamic equation for a chaotic pendulum in the Special Orthogonal Group SO(3) manifold, which is the foundation for our simulations.

Previously, till Phase I, we had successfully simulated and estimated the state of a chaotic pendulum.

1.4 Objectives of the Present Study

1. Mathematically Simulate Geometrically consistent models
 - (a) Chaotic Pendulum (3D Pendulum with a large swing angle) - This system will evolve on the configuration manifold $SO(3)$,
 - (b) Pendulum Cart System - This system will evolve on the configuration manifold $\mathbb{R}^2 \times SO(3)$, representing the combined space of two-dimensional translation and three-dimensional rotation.
 - (c) Duffing Oscillator - A second order non-linear differential oscillator evolving on S^2
 - (d) Double Pendulum - The double pendulum's configuration space is $\mathbb{R}^2 \times \mathbb{S}^2 \times \mathbb{S}^2$, where the first component represents translations in two-dimensional space and the subsequent components represent angles in two different planes.
2. State Estimation of aforementioned dynamical systems evolving on Riemannian Manifolds using Parallelizable Unscented Kalman Filter (UKF-M).

1.5 Organisation of the Thesis

The thesis has been organized, considering the overall path to achieve the final objective.

Chapter 1 primarily highlights the motivation behind carrying out the present work.

Chapter 2 covers a literature review related to Lie Algebra, Manifolds, Stochastic Ito

Calculus, and Kalman Filters. **Chapter 3** covers the methodology of the work. **Chapter**

4 consists of the results and conclusions, followed by a discussion of some future scopes.

Chapter 2

Background

This chapter will explore the mathematical concepts needed to understand the Parameter and State Estimation of random state variables of vibrating structures. We will start with Deterministic and Stochastic Dynamics in Euclidean Space, delve into Basic Manifold theory, and then build up on Kalman Filters and Apply the same to Manifolds. Meanwhile, we will learn how to formulate dynamics in manifolds and then study applying the filters to estimate the state of a system on Lie Groups.

2.1 Deterministic and Stochastic Dynamics

Deterministic dynamics refers to systems in which no randomness is involved in developing future states of the system. In other words, the future behavior of a deterministic system is entirely predictable based on its initial conditions and governing equations. These can be solved using the traditional techniques.

$$dX(t) = Adt \quad (2.1)$$

The system in which some amount of randomness is involved in the development of future states, this is generally done by introducing an additional quantity known as diffusion,

and the deterministic part known as the drift. Hence, Stochastic Differential Equations can be written as:

$$dX(t) = Adt + BdW_t \quad (2.2)$$

Here, A refers to the Drift term, the deterministic part of the considered Stochastic Differential Equation, and B refers to the diffusion or indeterministic or stochastic parts. The term dW_t is which introduces stochasticity in the given equation. It describes random motion proportional to a Brownian motion.

The solution of equation 2.2 cannot be solved using normal techniques as White noise (dW_t) is a non-continuous and non-differentiable process. To solve Stochastic Differential Equation like these, Ito-Calculus [6] is used

$$x(t) - x(t_0) = \int_{t_0}^t A dt + \int_{t_0}^t B dW_t \quad (2.3)$$

Where $\int_{t_0}^t B dW_t = \lim_{n \rightarrow \infty} \sum_{i=1}^n Bf(x_i^*, t_i^*)$ and $f(x_i^*, t_i^*) = W(t_{i+1}) - W(t_i)$

2.2 Lagrangian and Hamiltonian Dynamics on \mathbb{R}^n

The Lagrangian function, denoted as $L : T\mathbb{R}^n \rightarrow \mathbb{R}^1$, is a function that takes the configurations (generalized coordinates) and their time derivatives as inputs and returns a scalar value. It is commonly used in the Lagrangian mechanics framework to describe a physical system's dynamics.

Mathematically, the Lagrangian function can be expressed as the difference between the system's kinetic energy and potential energy, both of which are functions of the configurations. The kinetic energy is expressed in terms of the configurations and their time derivatives, while the potential energy is expressed solely in terms of the configurations.

In equation form, the Lagrangian function can be written as:

$$L(q, \dot{q}) = T(q, \dot{q}) - V(q) \quad (2.4)$$

where:

1. L represents the Lagrangian function.
2. q denotes the system's configurations (generalized coordinates).
3. \dot{q} represents the time derivatives of the configurations.
4. $T(q, \dot{q})$ is the system's kinetic energy, a function of the configurations and their time derivatives.
5. $V(q)$ is the system's potential energy, a function of the configurations.

The Lagrangian function plays a crucial role in Lagrangian mechanics, as it provides a concise and elegant formulation for deriving the equations of motion of a physical system. By applying the principle of least action, known as Hamilton's principle, the equations of motion can be derived by minimizing the action function associated with the Lagrangian function.

Using Hamilton's Variational Principle, the Euler-Lagrange Equation can be derived from this. The Euler-Lagrange Equation is given by:

$$\frac{d}{dt} \left(\frac{\partial L(q, \dot{q})}{\partial \dot{q}} \right) - \frac{\partial L(q, \dot{q})}{\partial q} = 0. \quad (2.5)$$

This gives us the Equation of Motion of the system under consideration.

We also look at the Hamiltonian Formulation as it helps us prove the symplectic nature of our numerical scheme[7].

In systems without randomness or uncertainty, the dynamics can be described using Hamiltonian formalism. In this framework, the Hamiltonian and the canonical equations are critical in determining the system's behavior.

The Hamiltonian, denoted as $\tilde{H}(q, p)$, is a function defined on the phase space $T * \mathbb{R}^n$,

which consists of the generalized coordinates q and their corresponding momenta p .

$$\tilde{H}(q, p) = p \cdot \dot{q} - L(q, \dot{q}) \Big|_{p=\frac{\partial L}{\partial \dot{q}}} \quad (2.6)$$

$$\frac{dq}{dt} = -\frac{\partial \tilde{H}}{\partial p}, \quad \frac{dp}{dt} = \frac{\partial \tilde{H}}{\partial q} \quad (2.7)$$

Together, the Hamiltonian and the canonical equations provide a complete and deterministic description of the dynamics in systems without any randomness or uncertainty. Solving these equations determines the evolution of the system's coordinates and momenta over time.

2.3 Manifolds

2.3.1 Definition

An abstract mathematical space known as a manifold has a structure that may be more complex globally but is similar to the Euclidean geometry-described spaces locally. For instance, the surface of the Earth is varied; although locally, it appears flat when seen globally from space, and it is rounded. It is possible to 'glue' various Euclidean spaces together to create a manifold [8]. A circle S^1 is an example of a manifold. Although a small portion of a circle resembles a slightly bent portion of a straight-line segment, the circle and the segment are two different 1D manifolds. A straight line segment can be bent, and the ends can be joined with glue to create a circle. Examples of 2D manifolds include the surfaces of a sphere and a torus. Manifolds are crucial components of mathematics, physics, and control theory because they enable the expression and comprehension of more complex structures in terms of the well-known characteristics of simpler Euclidean spaces.

Take into consideration a set M that is a potential manifold. Any point x on M has an associated Euclidean chart, which is given by a one-on-one mapping and plotted onto the map $\theta_i : M \rightarrow \mathbb{R}^n$, with an associated Euclidean image $V_i = \theta_i(U_i)$. Where U_i belongs

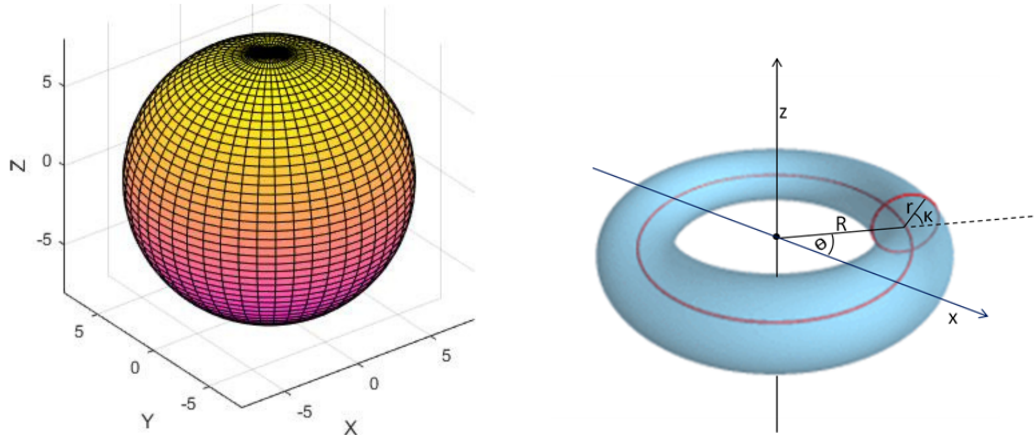


Fig. 2.1: Manifolds (a) Hypersphere (b) Torus

to M and $V_i \in \mathbb{R}^n$.

2.3.2 Notations

Numerous mathematical operations arise in the analysis and operations of manifolds. So, it is a good practice to fix all the notations that will be used to describe the mathematics in the further sections. M stands for a Riemannian manifold. The tangent space to the manifold M at a point $x \in M$ is designated as $T_x M$. The tangent bundle denoted by the symbol TM is defined as $TM := (x, v), x \in M, v \in T_x M$. A manifold is endowed with a local metric, and this local metric defines the local norm $\|V_x\| = \sqrt{(V \cdot V^T)}$ for $V \in T_x M$. The Riemannian gradient of a function $\psi : \mathbb{R} \rightarrow M$ evaluated at any point $x \in M$ is denoted as $\text{grad}_x \psi$. The covariant derivative of a vector field $w \in TM$ in the direction of $v \in T_x M$ is denoted by $\nabla_v w$. We assume M to be endowed with a metric connection. The parallel transport operator $P(x \rightarrow y)$ transports a tangent vector from $T_x M \rightarrow T_y M$. A manifold exponential map $\exp : TM \rightarrow M$ is applied as $\exp_x(v)$. Its inverse 'log' is defined locally and is denoted by $\log_{y,x}$ where y is the reference point $y \in M$. Given two points in the manifold M , the distance between them is denoted by $d(x, y)$, which is termed as the Riemannian distance between x and y . Having prepared a notation for all the objects, we define each of the terms individually.

Tensors

A tensor is an object that is invariant under a change of coordinates and has components that change in a special, predictable way under the change of coordinates. A tensor is a collection of vectors and co-vectors combined using the tensor product. Tensors follow two transformation rules:

- Forward Transformation (F):

$$T'_{ij} = \frac{\partial x'_i}{\partial x_k} \frac{\partial x'_j}{\partial x_l} T_{kl} \quad (2.8)$$

- Backward Transformation (B):

$$T_{kl} = \frac{\partial x_i}{\partial x'_k} \frac{\partial x_j}{\partial x'_l} T'_{ij} \quad (2.9)$$

such that $F \cdot B = I$.

Co-Vectors

A function that takes a vector and produces a scalar is called a co-vector. Spaces of co-vectors are called dual spaces. Co-vectors are invariant, but co-vector components are not invariant.

Metric Tensor

A metric tensor is an additional structure on a manifold M in the field of differential geometry that allows for the definition of distances and angles, much like the inner product on an Euclidean space does. A metric tensor on M is made up of metric tensors at each point $p \in M$ that vary smoothly with p , and a metric tensor at a point $p \in M$ is a bilinear form defined on the tangent space at p . Metric Tensor is one of the most critical objects in Manifolds as it is the metric tensor that allows us to do mathematical operations, such as finding the area, shortest distance, etc in manifolds. Consider the example of the

Pythagoras theorem, which finds us the hypotenuse distance in a triangle but is only valid in the orthonormal basis, so to do this in a manifold, we require a metric tensor.

There are two methods available to define the metric tensor. These are:

1. Intrinsic Approach: The manifold is not defined by the intrinsic view as enmeshed in another space. Instead, it defines it using a metric or other relevant data that informs us of curvature. This is also referred to as the "bug-eye view".
2. Extrinsic Approach: A manifold's extrinsic view is a portion of a larger space, typically one with more dimensions. In that case, the manifold can be described by an equation that indicates which points it takes up in the larger space. For instance, the unit sphere is seen as a subset of Euclidean 3-space when viewed extrinsically. This is also referred to as the "bird eye view".

Mathematically, a metric tensor is the inner product of the basis vectors of the manifold under consideration.

$$G = \begin{bmatrix} g_{ii} & g_{ij} \\ g_{ji} & g_{jj} \end{bmatrix} \quad (2.10)$$

Where, the components of the metric tensor are the inner products of the basis vectors in the intrinsic space, $g_{ij} = \mathbf{e}_i \cdot \mathbf{e}_j$. This is the intrinsic definition where the manifold under consideration is the sphere. In the case of extrinsic view, the metric tensor is defined as follows:

$$G = \begin{bmatrix} \mathbf{e}_x \cdot \mathbf{e}_x & \mathbf{e}_x \cdot \mathbf{e}_y & \mathbf{e}_x \cdot \mathbf{e}_z \\ \mathbf{e}_y \cdot \mathbf{e}_x & \mathbf{e}_y \cdot \mathbf{e}_y & \mathbf{e}_y \cdot \mathbf{e}_z \\ \mathbf{e}_z \cdot \mathbf{e}_x & \mathbf{e}_z \cdot \mathbf{e}_y & \mathbf{e}_z \cdot \mathbf{e}_z \end{bmatrix} \quad (2.11)$$

Where the \mathbf{e} basis vectors are from the Euclidean space, we can perform the operations on geometrical surfaces once this is established. The Metric Tensor is also called the First

Fundamental Form.

Geodesics

The straightest possible path we can draw on surfaces between two points is called a geodesic. A curve that minimizes length locally is a geodesic. It is, in effect, the path that a particle that is not accelerating would take. The geodesics are lines that are straight in the plane. The geodesics on the sphere are large circles. The Riemannian metric impacts the notions of distance and acceleration, which also affects the geodesics in space [9].

In addition to having many other intriguing qualities, geodesics maintain a direction on a surface. Any point on a geodesic arc has a normal vector that runs parallel to the surface. The Equation of Geodesic is given by:

$$\frac{d^2u^k}{d\lambda^2} + \Gamma_{ij}^k \frac{du^i}{d\lambda} \cdot \frac{du^j}{d\lambda} = 0 \quad (2.12)$$

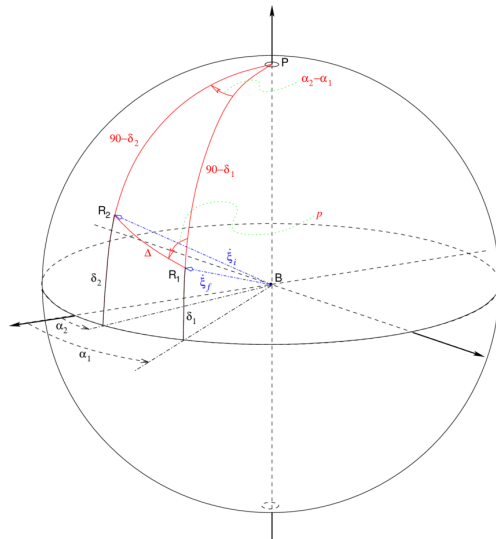


Fig. 2.2: Geodesic between two points on Sphere

Christoffel symbols

The Christoffel symbols are a set of numbers that represent the metric link between mathematics and physics. A metric can measure distances on surfaces or other manifolds thanks to the metric connection, a specialization of the affine connection. The Christoffel symbols illustrate how coordinates on the manifold relate to (pseudo-)Riemannian geometry. Then, more ideas, such as parallel transportation, geodesics, etc., can be expressed using Christoffel symbols. When there is some symmetry between the coordinate system and the metric tensor, many Christoffel symbols are zero. Below is a slight derivation of how a geodesic equation is obtained and the role of Christoffel symbols in the geodesics of a surface. Note that Einstein's Summation notation is followed. Methods to find the geodesic equation: We need to solve the equation.

$$\frac{d^2\vec{R}}{d\lambda^2} = \frac{d^2\vec{R}}{d\lambda^2}_{\text{tangential}} + \frac{d^2\vec{R}}{d\lambda^2}_{\text{normal}} \quad (2.13)$$

Now, Tangential Component = 0, on expanding the above equation we get,

$$\frac{d^2R_j}{d\lambda^2} = \left(\frac{d^2u^k}{d\lambda^2} + \Gamma_{ij}^k \frac{du^i}{d\lambda} \frac{du^j}{d\lambda} \right) \frac{\partial\vec{R}}{\partial u^k} + L_{ij} \frac{du^i}{d\lambda} \frac{du^j}{d\lambda} \hat{n} \quad (2.14)$$

$$\frac{d^2u^k}{d\lambda^2} + \Gamma_{ij}^k \frac{du^i}{d\lambda} \frac{du^j}{d\lambda} = 0 \quad (\text{Geodesic Equation}) \quad (2.15)$$

$$\Gamma_{ij}^k = \frac{\partial^2\vec{R}}{\partial u^j \partial u^i} \cdot \frac{\partial\vec{R}}{\partial u^l} g^{lk} \quad (\text{Christoffel Symbol}) \quad (2.16)$$

Here u^i and u^j are the basis vectors, and R is the position vector. And g^{lk} is the component of the inverse metric tensor.

Covariant Derivative

The covariant derivative in mathematics is a method of expressing a derivative along tangent vectors of a manifold. In contrast to the method provided by a primary connection on the frame bundle, the covariant derivative introduces and deals with a connection on a manifold through a differential operator [17].

Derivation: Suppose we have a vector field $A(x^i)$ Writing in terms of basis vectors

$$\begin{aligned} dA &= d(A^i de^i) \\ &= (dA^i)e^i + A^i(de^i) \\ &= \left(\frac{\partial A^i}{\partial x^j} dx^j \right) e^i + A^i \left(\frac{\partial e^i}{\partial x^j} dx^j \right) \\ &= \left(\frac{\partial A^i}{\partial x^j} dx^j \right) e^i + A^i \Gamma_{ij}^k e^k dx^j \\ &= \left(\frac{\partial A^i}{\partial x^j} + A^i \Gamma_{ij}^k \right) e^k dx^j \end{aligned}$$

Parallel Transport

Parallel transport is a technique used in geometry to move geometrical information along a manifold's rounded curves. If the manifold has an affine connection, one can move its vectors along curves while maintaining their parallelism about the connection. Thus, the parallel transport for a connection provides a means of connecting the geometries of close-by points or, in specific ways, moving the local geometry of a manifold along a curve. There may be other parallel transport concepts, but this definition only refers to one method of joining the geometries of points on a curve. In actuality, parallel transport is the infinitesimal analog of the conventional notion of connection. The connection here is referred to as the covariant derivative.

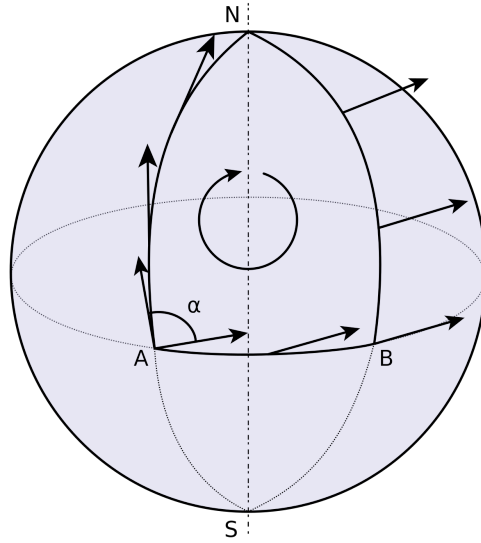


Fig. 2.3: Parallel transport of a vector in a manifold

The notion of covariant derivative is closely tied to parallel transport along a curve. The parallel transport operator $P_{x \rightarrow y}^r : T_{\gamma(x)} M \rightarrow T_{\gamma(y)} M$ associated with the curve $\gamma : I \rightarrow M$ with $\theta \in I$, $\gamma(0) = x'$, and $u, w \in T_{x'} M$ is given by

$$G_{\gamma(t)}(P_{0 \rightarrow t}^r \gamma(v), P_{0 \rightarrow t}^r \gamma(w)) = G_{x'}(u, w) \quad (2.17)$$

The covariant derivative of a vector field $E \in X(M)$ in the direction ω is related to the parallel transport operator by

$$\nabla_\omega E = \left. \frac{d}{dt} P_{\epsilon \rightarrow 0}^t E(\gamma(t)) \right|_{t=0} \quad (2.18)$$

If vector field E satisfies the condition $P_{\epsilon \rightarrow 0}^t E(\gamma(x)) = E(\gamma(y))$, the field \vec{t} is said to be parallel along r . The parallelism term for covariant derivative is $\nabla_{\dot{\gamma}} E = 0$.

A geodesic in manifold M with connection ∇ and associated parallel translation operator P_G , is a curve γ such that $\dot{\gamma}$ is parallel translated along r itself.

$$P_{G_s \rightarrow \gamma}^t (\dot{\gamma}(s)) = \dot{\gamma}(t) \quad (2.19)$$

Exponential Mapping

In Riemannian geometry, an exponential map refers to a mapping from a subset of the tangent space $T_p M$ of a Riemannian manifold M to the manifold itself. This exponential map is determined by the canonical affine connection established by the Riemannian metric.

The geodesic equation, given by [17]

$$\ddot{x}^k + \sum_{i,j} \Gamma_{ij}^k(\gamma) \dot{x}^i \dot{x}^j = 0 \quad (2.20)$$

Describes the behavior of geodesics on the manifold. For any vector V in $T_x M$, there exists an interval I around the origin O and a unique geodesic $\gamma(t, x) : I \rightarrow M$ such that $\gamma(0) = x$ and $\dot{\gamma} = v$. The exponential map, denoted as $\exp : T_x M \rightarrow M$, maps each vector v in the tangent space to a point on the manifold, denoted as $\exp_x v$, given by $\gamma(1; x, v)$.

A manifold M is geodesically complete if the domain of the exponential map, denoted as Exp , covers the entire tangent space $T_x M$ for every x in M .

Logarithmic Mapping

In Riemannian geometry, it is the inverse of the exponential mapping, such that it returns a vector which belongs to the tangent space of M which is the direction vector between two point in the manifold.

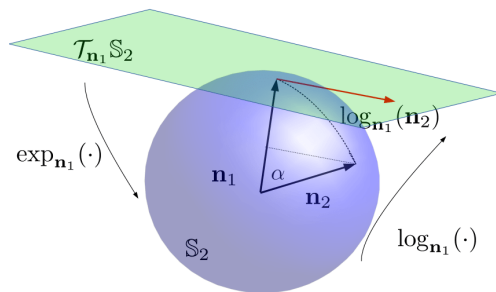


Fig. 2.4: Exponential Mapping and Logarithmic Mapping on surface of S^2 manifold

2.4 Lie Groups and Lie Algebras

A Lie group is a smooth manifold that also carries a group structure whose product and inversion operations are smooth as maps of manifolds. These structures naturally appear when describing physical symmetries.

A Lie group[10][11] is a group whose elements can have a continuous real number parametrization, like the rotation group $SO(3)$, which can have the Euler angles as its parametrization. An analytic real or complex manifold that is also a group, such that the group operations multiplication and inversion are analytic maps, is referred to as a Lie group in a more formal sense.

2.4.1 Group Axioms

1. **Closure:** If $a, b \in G$, then $\phi(a, b) \in G$.
2. **Associative:** If $a, b, c \in G$, then $\phi(a, \phi(b, c)) = \phi(\phi(a, b), c)$.
3. **Identity:** If $a \in G$, then there exists $e \in G$ such that $\phi(a, e) = \phi(e, a) = a$.
4. **Inverse:** If $a \in G$, then there exists a unique element $a^{-1} \in G$ such that $\phi(a, a^{-1}) = \phi(a^{-1}, a) = e$.

2.4.2 Lie Group

A Lie group is a smooth manifold M with a group G structure concurrently consistent with its manifold M structure in group multiplication and group inversion. The group identity element is a point e at G . Every point of the manifold in a Lie group has the same appearance, so every tangent space at every moment is the same. The group structure mandates that each element's composition stays on the manifold and that each component also has an inverse in the manifold. Calculus on groups is possible thanks to Lie groups, which connect the local characteristics of smooth manifolds.

2.4.3 Group Actions

Lie groups can alter the elements of other sets, leading to transformations such as rotations, translations, scaling, and combinations thereof. A valid group action must satisfy the axioms of identity and compatibility.

2.4.4 Lie Algebra

If we have a point $X(t)$ that moves on a manifold M associated with a Lie group, the velocity of this point belongs to the tangent space of the manifold, denoted as $T_x M$. The smoothness of the manifold ensures the presence of a unique tangent space at each point. The tangent space at the Lie group's identity element is known as that particular group's Lie algebra. It is important to note that every Lie group is accompanied by its corresponding Lie algebra.

2.4.5 Exponential Map and Logarithmic Map

The exponential map is a mapping that establishes a diffeomorphism between the Lie algebra and the Lie group. It allows us to convert elements from the Lie algebra to corresponding elements in the Lie group. Conversely, the inverse of the exponential map is the logarithmic map, enabling us to return to the Lie algebra from the Lie group.

In our research, calculating the exponential mapping directly poses challenges as it necessitates a deep understanding of advanced concepts in Differential Geometry. As a result, we opt for a shortcut by leveraging the action exerted by Lie groups on the configuration manifold considered in our study. This approach provides us with a more accessible way to incorporate the effects of Lie groups in our analysis.

Rotational Lie Groups

This group is the subset of the General Linear Group whose Group Action represents the rotations induced in any physical system. The Rotational Groups are $n \times n$ matrices where

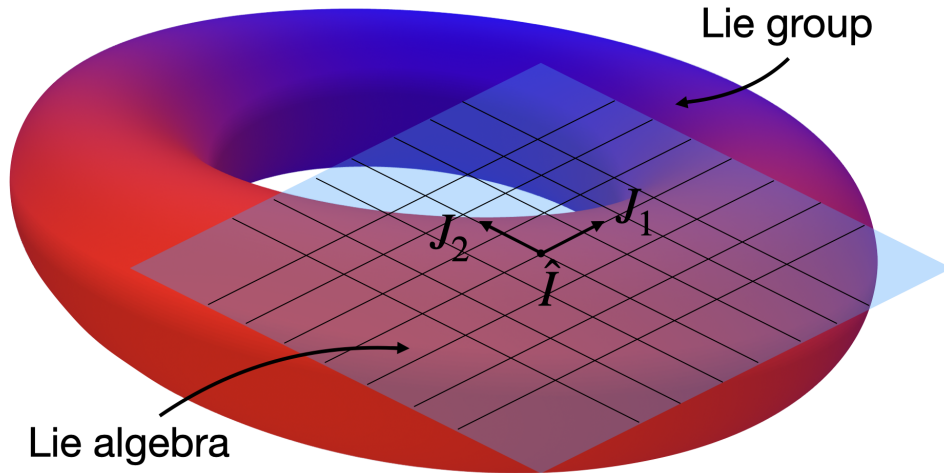


Fig. 2.5: Working of Lie Groups and Lie Algebra

n is the number of rotation axes. The Rotational group may have n dimensions, but the rotations in 2 and 3 dimensions are essential.

Uni-axial Rotation Groups or $SO(2)$

The following transformation of the joint coordinates results from the uniaxial joint rotation in a single Cartesian plane around a perpendicular axis, for example, the $x - y$ plane about the z axis with rotation angle θ :

$$SO(2) = \begin{bmatrix} \cos \theta & -\sin \theta \\ \sin \theta & \cos \theta \end{bmatrix} \quad (2.21)$$

Lie Algebra:

$$\mathfrak{so}(2) = \left\{ \begin{bmatrix} 0 & -t \\ t & 0 \end{bmatrix}, \quad t \in \mathbb{R} \right\} \quad (2.22)$$

Exponential Map:

$$\exp \left(\begin{bmatrix} 0 & -\theta \\ \theta & 0 \end{bmatrix} \right) = \gamma_\theta(1) = \begin{bmatrix} \cos t\theta & -\sin t\theta \\ \sin t\theta & \cos t\theta \end{bmatrix} \quad (2.23)$$

Three-axial Rotation Groups or $SO(3)$

The group $SO(3)$ comprises rotation matrices or special orthogonal matrices in 3D space subject to matrix multiplication. In all groups, SO , inversion, and composition are accomplished through transposition and product (n). The lie algebra of the group is defined by angular velocities $\omega_x, \omega_y, \omega_z$.

$$[\omega] = \begin{bmatrix} 0 & -\omega_z & \omega_y \\ \omega_z & 0 & -\omega_x \\ -\omega_y & \omega_x & 0 \end{bmatrix} \quad (2.24)$$

Exponential Map:

$$R = \exp([\omega]\theta) \in SO(3), \text{ where } R \text{ is the rotation matrix.} \quad (2.25)$$

$$R = I + [\omega] \sin(\theta) + [\omega]^2 (1 - \cos(\theta)) \quad (2.26)$$

Logarithm:

$$\theta[\omega] = \log(R)\theta(R - R^\top) \frac{1}{2} \sin(\theta) \quad (2.27)$$

Where,

$$\theta = \cos^{-1} \left(\frac{\text{trace}(R) - 1}{2} \right) \quad (2.28)$$

2.5 Kalman Filter

The Kalman filter[12] is a linear recursive algorithm that estimates the state of a dynamic system from a series of noisy measurements. It is widely used for state estimation in various fields, including control systems and robotics, where systems are linear and both process and Gaussian with known covariance matrices. To extend the same for non-linear systems, we either linearize the system using Taylor Series Expansion as done in Extended Kalman Filter(EKF) or use deterministic sampling, i.e., unscented transform for propagation of mean and covariance through non-linear systems[13]. When dealing with systems evolving on manifolds, such as rotations or orientations, we incorporate Lie Group Theory and then use the Unscented Kalman Filter on Manifolds[14].

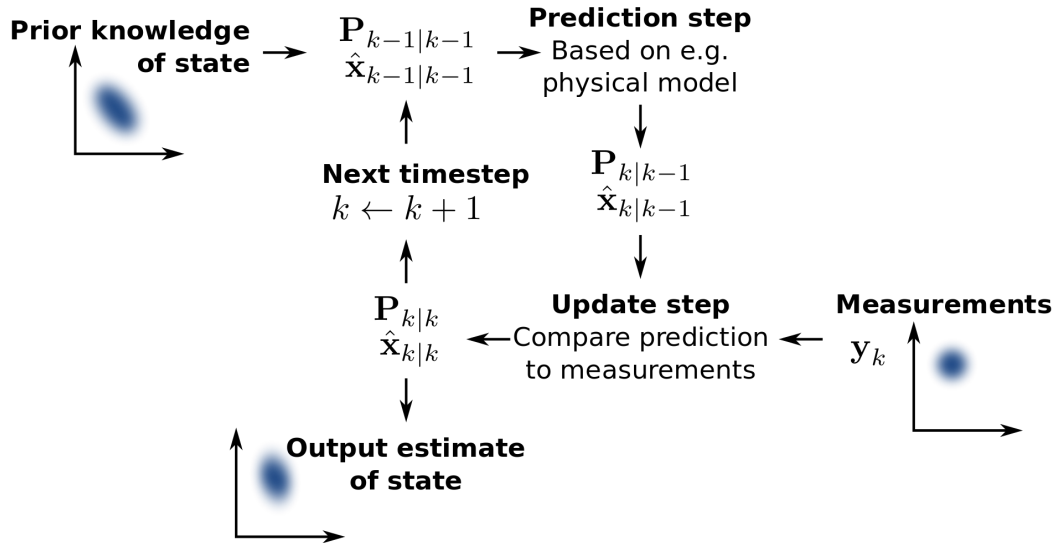


Fig. 2.6: Basic Principle of Kalman Filter

2.5.1 Mathematical Background: Kalman Filter

Consider a dynamic system evolving on a manifold \mathbb{M} with state $x \in \mathbb{M}$. The state evolves according to a dynamic model, and measurements z related to the state are obtained with noise. The Kalman filter formulates the state estimation problem using the following equations:

- **State Prediction:** The predicted state is obtained from the system dynamics:

$$\hat{x}_{k|k-1} = f(\hat{x}_{k-1|k-1}, u_{k-1}) \quad (2.29)$$

where f is the state transition function, $\hat{x}_{k|k-1}$ is the predicted state, $\hat{x}_{k-1|k-1}$ is the previous state estimate, and u_{k-1} is the control input.

- **Error Covariance Prediction:** The error covariance matrix is predicted using the Jacobian of the state transition function:

$$P_{k|k-1} = A_{k-1} P_{k-1|k-1} A_{k-1}^\top + Q_{k-1} \quad (2.30)$$

where A_{k-1} is the Jacobian of f for the state, $P_{k-1|k-1}$ is the error covariance matrix of the previous estimate, and Q_{k-1} is the process noise covariance.

- **Measurement Prediction:** The predicted measurement is obtained using the measurement model:

$$\hat{z}_{k|k-1} = h(\hat{x}_{k|k-1}) \quad (2.31)$$

where h is the measurement function.

- **Kalman Gain Calculation:** The Kalman gain is computed to determine the weight of the measurement in the state correction:

$$K_k = P_{k|k-1} H_k^\top (H_k P_{k|k-1} H_k^\top + R_k)^{-1} \quad (2.32)$$

H_k is the Jacobian of the measurement function, and R_k is the measurement noise covariance.

- **State Update:** The state is updated based on the measurement and the Kalman

gain:

$$\hat{x}_{k|k} = \hat{x}_{k|k-1} + K_k(z_k - \hat{z}_{k|k-1}) \quad (2.33)$$

- **Error Covariance Update:** The error covariance matrix is updated using the Kalman gain:

$$P_{k|k} = (I - K_k H_k) P_{k|k-1} \quad (2.34)$$

where I is the identity matrix.

2.5.2 Unscented Kalman Filter on Euclidean Spaces

UKF is a non-linear state estimation technique that extends the essential Kalman Filter. Instead of linearizing the system dynamics and measurement models, the UKF employs a deterministic sampling technique to propagate the mean and covariance through non-linear functions. UKF has several advantages, including 1) the expected error is lower than the EKF, 2) the new filter can be applied to non-differentiable functions, 3) the new filter avoids the derivation of Jacobian matrices, and 4) the new filter is valid to higher-order expansions than the standard EKF. The UKF works on the premise that it should be easier to approximate a Gaussian distribution with a fixed number of parameters than an arbitrary nonlinear function. The Unscented Transform approximates the mean and covariance of a nonlinear function of random variables. It propagates sigma points through non-linear functions while preserving the mean and covariance of the distribution. Sigma points are selected symmetrically around the mean, often along the principal axes of the distribution.

$$x_{k+1} = f(x_k, k) + w_k \quad (2.35)$$

$$\tilde{y}_k = h(x_k, k) + v_k \quad (2.36)$$

Note that a continuous-time model can always be written using equation (2.35) through an appropriate numerical integration scheme. It is assumed that w_k and v_k are zero-mean Gaussian noise processes with covariances given by Q_k and R_k , respectively. We first rewrite the Kalman filter update equations as:

$$\hat{x}_k^+ = \hat{x}_k^- + K_k v_k \quad (2.37)$$

$$P_k^+ = P_k^- - K_k P_{vv} K_k^\top \quad (2.38)$$

where v_k is the innovations process, given by:

$$v_k \equiv \tilde{y}_k - \hat{y}_k^- = \tilde{y}_k - h(\hat{x}_k^-, k) \quad (2.39)$$

The covariance of v_k is defined by P_{vv} . The gain K_k is computed by:

$$K_k = P_{xy,k} (P_{vv,k})^{-1} \quad (2.40)$$

where $P_{xy,k}$ is the cross-correlation matrix between \hat{x}_k^- and \hat{y}_k^- .

The Unscented filter uses a different propagation than the form given by the standard extended Kalman filter. Given an $n \times n$ covariance matrix P , a set of order n points can be generated from the columns (or rows) of the matrices $\pm\sqrt{n}P$. The set of points is zero-mean, but if the distribution has mean μ , then simply adding μ to each of the points yields a symmetric set of $2n$ points having the desired mean and covariance. Due to the symmetric nature of this set, its odd central moments are zero, so its first three moments are the same as the original Gaussian distribution.

Formulation of Sigma Points

The general formulation for the propagation equations is given as follows. First, the following set of sigma points[15] is computed:

$$\sigma_k \leftarrow 2n \text{ columns from } \pm \gamma \sqrt{P_k^+ + \bar{Q}_k} \quad (2.41)$$

$$\chi_k(0) = \hat{x}_k^+ \quad (2.42)$$

$$\chi_k(i) = \sigma_k(i) + \hat{x}_k^+ \quad (2.43)$$

Where the matrix \bar{Q}_k is related to the process noise covariance, which will be discussed shortly. The parameter γ is given by:

$$\gamma = \sqrt{n + \lambda} \quad (2.44)$$

where the composite scaling parameter, λ , is given by

$$\lambda = \alpha^2(n + \kappa) - n \quad (2.45)$$

The constant α determines the spread of the sigma points and is usually set to a small positive value (e.g., $1 \times 10^{-4} \leq \alpha \leq 1$). Also, the significance of the parameter κ will be discussed shortly. One efficient method to compute the matrix square root is the Cholesky decomposition. Alternatively, the sigma points can be chosen to lie along the eigenvectors of the covariance matrix. Note that there are a total of $2n$ values for σ_k (the positive and negative square roots). The transformed set of sigma points is evaluated for each of the points by

$$\chi_{k+1}(i) = f[\chi_k(i), k] \quad (2.46)$$

Intrinsic Statistics on Euclidean Spaces

Expectation:

$$\mathbb{E}(g(X)) = \int_{\mathbb{R}} g(x)f(x) dx \quad (2.47)$$

Variance:

$$V(X) = \mathbb{E} (X - \mathbb{E}(X))^2 \quad (2.48)$$

Covariance:

$$\text{COV}(X, Y) = \mathbb{E} [(X - \mathbb{E}(X)) \cdot (Y - \mathbb{E}(Y))] \quad (2.49)$$

We now define the following weights:

$$W_{\text{mean}}^0 = \frac{\lambda}{n + \lambda} \quad (2.50)$$

$$W_{\text{cov}}^0 = \frac{\lambda}{n + \lambda} + (1 - \alpha^2 + \beta) \quad (2.51)$$

$$W_{\text{mean}}^i = W_{\text{cov}}^i = \frac{1}{2(n + \lambda)}, \quad i = 1, 2, \dots, 2n \quad (2.52)$$

where β is used to incorporate prior knowledge of the distribution (a good starting guess is $\beta = 2$). The predicted mean for the state estimate is calculated using a weighted sum of the points $\chi_{x,k+1}(i)$, which is given by

$$\hat{x}_{-k+1} = \sum_{i=0}^{2n} W_{\text{mean}}^i \chi_{k+1}(i) \quad (2.53)$$

The predicted covariance is given by

$$P_{-k+1} = \sum_{i=0}^{2n} W_{\text{cov}}^i [\chi_{k+1}(i) - \hat{x}_{-k+1}] [\chi_{k+1}(i) - \hat{x}_{-k+1}]^\top + \bar{Q}_k \quad (2.54)$$

The mean observation is given by

$$\tilde{y}_{-k+1} = \sum_{i=0}^{2n} W_{\text{mean}}^i \gamma_{k+1}(i) \quad (2.55)$$

where

$$\gamma_{k+1}(i) = h[\chi_{k+1}(i), k+1] \quad (2.56)$$

The output covariance is given by

$$P_{yy,k+1} = \sum_{i=0}^{2n} W_{\text{cov}}^i [\gamma_{k+1}(i) - \tilde{y}_{-k+1}] [\gamma_{k+1}(i) - \tilde{y}_{-k+1}]^\top \quad (2.57)$$

Then, the innovations covariance is simply given by

$$P_{vv,k+1} = P_{yy,k+1} + R_{k+1} \quad (2.58)$$

Finally, the cross-correlation matrix is determined using

$$P_{xy,k+1} = \sum_{i=0}^{2n} W_{\text{cov}}^i [\chi_{k+1}(i) - \hat{x}_{-k+1}] [\gamma_{k+1}(i) - \tilde{y}_{-k+1}]^\top \quad (2.59)$$

The filter gain is then computed using equation (2.40), and the state vector can now be updated using equation (2.37). Even though propagations on the order of $2n$ are required for the Unscented filter, the computations may be comparable to the extended Kalman filter (especially if the continuous-time covariance equation needs to be integrated and a numerical Jacobian matrix is evaluated).

2.5.3 Unscented Kalman Filter on Riemannian Manifolds

Similar to defining UKF on Euclidean Spaces, we have first to develop Riemannian extensions of some fundamental concepts of the UKF theory, e.g., extensions of σ -representation, Unscented Transformation, noise, and statistics inclusion, and relations between their UKFs for Riemannian systems.[16]

Riemannian σ -Representation

In this section, first, we define Riemannian σ -representations (Ri σ R). They extend σ Rs to Riemannian manifolds: σ Rs approximate random vectors and Ri σ Rs approximate Riemannian random points.

Assumptions for Ri σ R:

1. all Riemannian manifolds are geodesically-complete
2. all Riemannian exponential mappings are defined with their domain, allowing them to realize diffeomorphisms;
3. every set of weighted points belonging to a Riemannian manifold admits one, and only one, Riemannian sample mean.

For the point $a \in \mathbb{N}$ and the natural numbers $l \geq 2$ and $N \geq 1$, consider i) a random point $X \sim (X, M_{a,2}^X, X, \dots, M_{a,l}^X, X)_n^N$ and ii) a weighted set $\chi := \{\chi_i, w_{m,i}, w_{c,j,i}, w_{cc,j,i} | \chi_i \in \mathbb{N}\}_{i=1}^N$ with sample mean μ_χ and sample moments $M_j^\chi, j = 2, \dots, l$.

Intrinsic Statistics for Riemannian Manifold

Expectation:

$$\mathbb{E}[\phi(X)] = \int_M \phi(y) p_X(y) dM(y) \quad (2.60)$$

Variance:

$$\sigma_X^2(y) = \int_M \text{dist}(y, z)^2 p_X(z) dM(z) \quad (2.61)$$

Covariance:

$$\Sigma_{XX} = \mathbb{E} \left[\overrightarrow{XX} - \overrightarrow{X} \overrightarrow{X}^T \right] \quad (2.62)$$

RIEMANNIAN UNSCENTED TRANSFORMATIONS

The concept of a *sigma* representation is a requisite for defining the UT. Essentially, a UT is an approximation of the joint PDF of two functionally-related random vectors X and

$Y = f(X)$ by two weighted sets χ with points χ_i and γ with points $\gamma_i = f(\chi_i)$, where χ is a σ -representation of X . For a Riemannian extension of the UT, we develop likewise.

Consider two Riemannian manifolds M and N , the function $f : U \subset M \rightarrow N$, the Riemannian random point $X \sim (X, M_X^2, \dots, M_X^l)_M$ taking values on M , and the sets:

$$\chi := \{\chi_i, w_{(m)i}, w_{(m^2\lambda_1\lambda_2)i}, \dots, w_{(m^l\lambda_1\dots\lambda_l)i}\}_{i=1}^N,$$

and

$$\gamma := \{\gamma_i, w_{(m)i}, w_{(m^2\lambda_1\lambda_2)i}, \dots, w_{(m^l\lambda_1\dots\lambda_l)i}\}_{i=1}^N,$$

where $\chi_i \in M$, $w_{(m^2\lambda_1\lambda_2)i}, \dots, w_{(m^l\lambda_1\dots\lambda_l)i} > 0$, and $\gamma_i = f(\chi_i)$.

If χ is an *RilthσR* of X , then the l th order Riemannian Unscented Transformation (*RilUT*) is defined by:

$$RilUT(f, X, M_X^2, \dots, M_X^l) := h(\mu_\gamma, M_\gamma^2, \dots, M_\gamma^l, M_{\lambda_1\lambda_2}^2, \dots, M_{\lambda_1\dots\lambda_l}^l).$$

If $l = 2$ or l is irrelevant for a given discussion, we can omit the reference to l and write $RiUT := RI2UT$.

The update equations on the UKF on manifolds become [17][16]

$$G_k = P_{\hat{k}|k-1}^{xy} \left(P_{\hat{k}|k-1}^{yy} \right)^{-1}, \quad (2.63)$$

$$\hat{x}_{k|k} = \hat{x}_{k|k-1} + G_k (y_k - \hat{y}_{k|k-1}), \quad (2.64)$$

$$P_{k|k}^{xx} = P_{k|k-1}^{xx} - G_k P_{\hat{k}|k-1}^{xy} (G_k)^T. \quad (2.65)$$

2.6 Unscented Kalman Filter on Lie Groups

Given the complexity of defining σ point and then calculating the state update for systems evolving in complex manifolds, we can use the idea of Exponential and Logarithmic mapping to transform back and forth between vector and its projection on the Manifold and Tangent

Space, respectively and then apply UKF based on Tangent Space because of the property of Lie Group to act as Euclidean Space for small perturbations around Identity.

2.7 Summary

In this chapter, we covered the fundamental concepts necessary for grasping the essentials of Manifolds and Kalman Filters. Additionally, we explored the workings of Lie Groups, mainly focusing on Rotational Lie Groups, which will play a crucial role in our formulation. Before delving into the formulation, we will establish the methodology for expressing dynamics on manifolds. The subsequent chapter will introduce the formulation of the filter, explicitly emphasizing the Spherical Manifold.

Chapter 3

State Estimation on Manifolds

In this chapter, we explore the application of the Unscented Kalman Filter (UKF) on parallelizable manifolds to estimate the dynamics of systems evolving on two-sphere manifold(S^2)[14].

3.1 Problem Formulation

The set of all points in the Euclidean space \mathbb{R}^3 , lying on the surface of the unit ball about the origin, belongs to the two-sphere manifold, denoted as $S^2 = \{x \in \mathbb{R}^3 | \|x\|_2 = 1\}$. Systems such as a spherical pendulum evolve on the two-sphere manifold. So, we first simulate models on S^2 and $SO(3)$ manifolds using numerical techniques like the Geometric Ito-Taylor 1.5 Method[5]. This method accurately represents the system's behavior, accounting for both deterministic and stochastic components. The numerical integration process involves discretizing the time domain and updating the state variables (angular velocity and orientation) at each time step.

By following this data generation process, we can simulate the behavior of structures equipped with geometrically consistent tuned mass dampers under various conditions, allowing us to investigate state estimation and then thus design a filter.

3.2 Spherical Pendulum

A spherical pendulum consists of a rigid link connected to a frictionless, two-degree-of-freedom ideal pivot; the mass of the spherical pendulum is assumed to be concentrated at the end of the massless link. The spherical pendulum acts under uniform, constant gravity, and no other force acts on it.

Euler–Lagrange Equations in Terms of (q, \dot{q})

The Lagrangian function $L : TS^2 \rightarrow \mathbb{R}^1$ for a spherical pendulum[18] can be written as the difference between the kinetic energy function and the gravitational potential energy function:

$$L(q, \dot{q}) = \frac{1}{2}mL^2\|\dot{q}\|^2 - mgLe_3^T q. \quad (3.1)$$

The Euler–Lagrange equation for the spherical pendulum is obtained from (2.5) as

$$mL^2\ddot{q} + mL^2\|\dot{q}\|^2q + mgL(I_{3\times 3} - qq^T)e_3 = 0. \quad (3.2)$$

This equation describes the Lagrangian dynamics of the spherical pendulum in terms of $(q, \dot{q}) \in TS^2$ on the tangent bundle of the configuration manifold.

Euler–Lagrange Equations in Terms of (q, ω)

A convenient form of the Euler–Lagrange equations can also be obtained in terms of the angular velocity vector of the spherical pendulum $\omega \in T_qS^2$, which satisfies the rotational kinematics

$$\dot{q} = S(\omega)q. \quad (3.3)$$

The angular velocity vector satisfies $\omega^T q = 0$, and $S(\omega)$ is the 3×3 skew-symmetric matrix function.

The modified Lagrangian function can be expressed in terms of the angular velocity

vector of the spherical pendulum as

$$\tilde{L}(q, \omega) = \frac{1}{2}mL^2\|\omega\|^2 - mgLe_3^T q. \quad (3.4)$$

The Euler–Lagrange equation, expressed in terms of the angular velocity vector, consists of the rotational kinematics (3.3) and the equation obtained from (2.5).

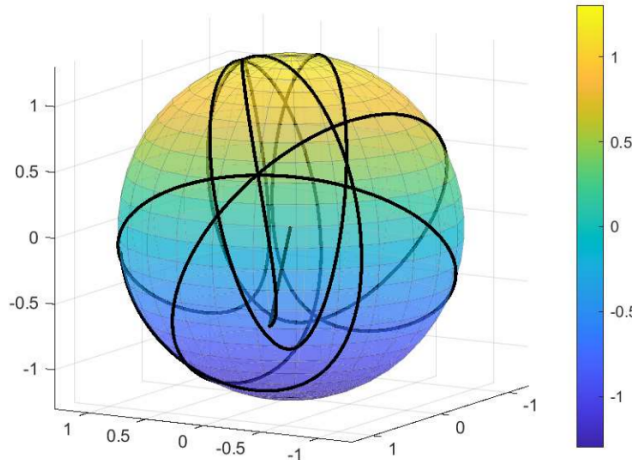


Fig. 3.1: Trajectory of Bob of a Spherical Pendulum

3.3 Pendulum Cart System

The dynamics of a spherical pendulum under constant gravitational force attached to the center of mass of a cart that translates on a frictionless horizontal plane is considered. The spherical pendulum is assumed to be composed of a thin, massless rigid rod whose outboard end has a concentrated mass, and the other end is attached to the cart through a spherical joint or pivot. The cart is modeled as a spring-mass-dashpot[19] system. The system configuration is provided in Fig. 4. The mass of the cart and the pendulum are considered to be M and m , respectively, with the pendulum’s length defined as l . The stiffness for the cart is denoted by k and c is the damping coefficient of the dashpot. Accordingly,

the configuration of the underlying system is described by $(q, x) \in S^2 \times \mathbb{R}^2$, such that the dynamics lie on the manifold given by $S^2 \times \mathbb{R}^2$.

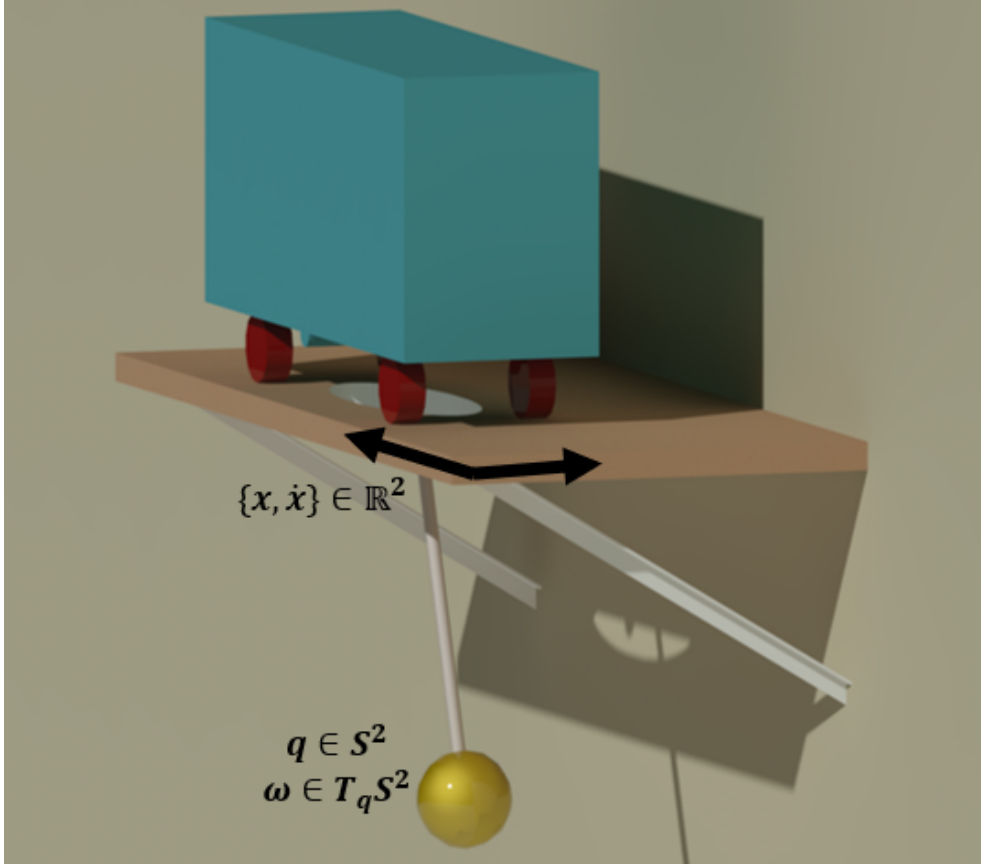


Fig. 3.2: Schematic Representation of Pendulum Cart System

Since the position of the center of mass of the cart is given by $x \in \mathbb{R}^2$, its location in the inertial frame is obtained by a 3×2 matrix C , such that $Cx \in \mathbb{R}^3$. The matrix C is given as,

$$C = \begin{pmatrix} 1 & 0 \\ 0 & 1 \\ 0 & 0 \end{pmatrix}$$

Similarly, the center of mass of the mass element of the spherical pendulum is projected in the inertial frame using the following expression,

$$\mathbf{x}_l = \mathbf{Cx} + l\mathbf{q} \quad (3.5)$$

where $\mathbf{x}_l \in \mathbb{R}^3$. The total kinetic energy of the pendulum cart system in the inertial frame is defined as,

$$T(q, x, \dot{q}, \dot{x}) = \frac{1}{2}M\dot{x}^2 + \frac{1}{2}m\dot{x}_l^2 \quad (3.6)$$

the first term on the right-hand side of Eq. (2) is the cart's kinetic energy, and the second term denotes the kinetic energy of the mass element defining the spherical pendulum. Incorporating Eq. (1) in the above equation leads to

$$T(q, x, \dot{q}, \dot{x}) = \frac{1}{2}(Mc + m)\dot{x}^2 + \frac{1}{2}mlx^T \mathbf{C}^T \dot{q} + \frac{1}{2}ml\dot{q}^T \mathbf{C} \dot{x} + \frac{1}{2}ml^2\dot{q}^2 \quad (3.7)$$

The potential energy of the system is composed of the potential energy of the spherical pendulum due to gravity and the spring element of the cart, given as,

$$U(q, x) = mg\mathbf{e}_3^T q + \frac{1}{2}kx^2 \quad (3.8)$$

Here, \mathbf{e}_3 is the standard basis vector in \mathbb{R}^3 . Finally, the Lagrangian function defined on $L : TqS^2 \times \mathbb{R}^2 \rightarrow \mathbb{R}^1$ is written as,

$$L(q, x, \dot{q}, \dot{x}) = \frac{1}{2}(Mc + m)\langle \dot{x}, \dot{x} \rangle + mlx^T \mathbf{C}^T \dot{q} + \frac{1}{2}ml^2\langle \dot{q}, \dot{q} \rangle - mg\mathbf{e}_3^T q - \frac{1}{2}k\langle x, x \rangle \quad (3.9)$$

As $\dot{q} = \omega \times q$, the modified Lagrangian function in terms of the angular velocity vector ω can be expressed using the wedge operator as,

$$\hat{L}(q, x, \omega, \dot{x}) = \frac{1}{2}(Mc + m)\langle \dot{x}, \dot{x} \rangle - mlx^T \mathbf{C}^T \omega + \frac{1}{2}ml^2\langle \omega, \omega \rangle - mg\mathbf{e}_3^T q - \frac{1}{2}k\langle x, x \rangle \quad (3.10)$$

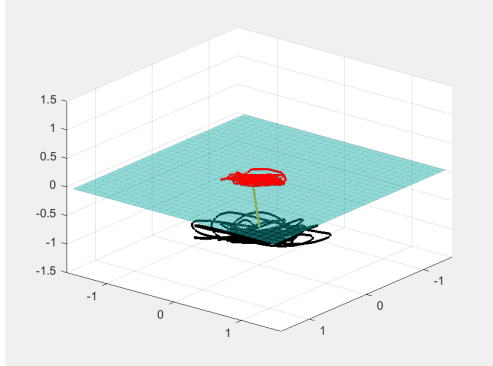


Fig. 3.3: Pendulum Cart Simulation.

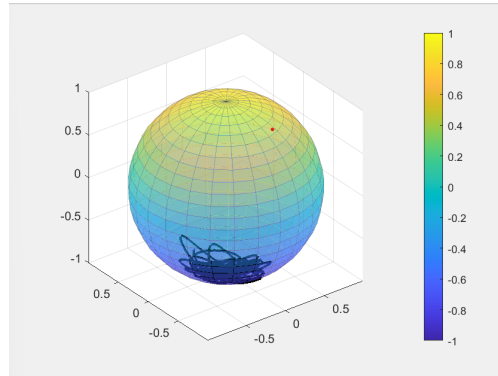


Fig. 3.4: Pendulum cart Trajectory.

3.4 Duffing Oscillator

The Duffing oscillator is a non-linear second-order differential equation used to model the motion of a damped oscillator with a more complex potential than in simple harmonic motion [20]. In physical terms, it models, for example, a spring pendulum whose spring's stiffness does not strictly obey Hooke's law. An extension of the Duffing potential reads[21]:

$$V_{\text{duf}} := \pm \frac{1}{2}d^2(x, r) \pm \frac{1}{4}\kappa d^4(x, r), \quad (3.11)$$

where again $d(\cdot, \cdot)$ denotes the Riemannian (geodesic) distance on the manifold M , $\kappa > 0$ is a free parameter, and $r \in M$ denotes a reference point. The signs \pm were introduced to account for the hard, the soft, and the double-well Duffing oscillator.

The Riemannian gradient of Duffing potentials corresponding to different combinations of signs reads:

$$\text{grad}_x V_{\text{duf}} = [\mp 1 \mp \kappa d^2(x, r)] \log_x(r). \quad (3.12)$$

The potential vanishes when $x = r$, but in the case of mixed signs, it also vanishes at every point $x \in M$ such that $d(x, r) = d_b$; therefore, this system presents infinitely many critical

points. Namely, we may define a set

$$C_{\text{duf}} := \{x \in M \mid d(x, r) = \sqrt{d_b}\} \quad (3.13)$$

of critical points in M .

Therefore, the dynamical system associated with a Duffing potential reads:

$$\begin{cases} \dot{x} = v, \\ \nabla_v v = -\mu\kappa\|v\|^{2(\varepsilon-1)}xv + \begin{cases} [1 + \kappa d^2(x, r)] \log_x(r), & \text{for the hard Duffing,} \\ [-1 - \kappa d^2(x, r)] \log_x(r), & \text{for the soft Duffing,} \\ [-1 + \kappa d^2(x, r)] \log_x(r), & \text{for the double-well Duffing.} \end{cases} \end{cases} \quad (3.14)$$

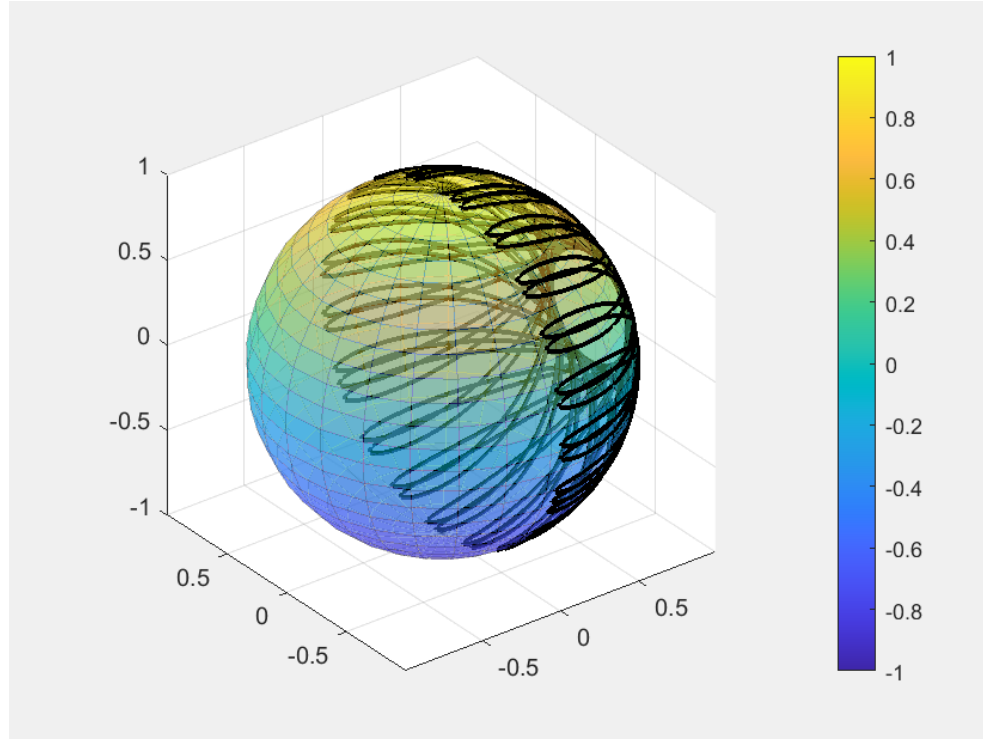


Fig. 3.5: Duffing Oscillator Trajectory

3.5 Double Pendulum

3.5.1 Euler–Lagrange Equations in Terms of (q, \dot{q})

The total kinetic energy is the sum of the kinetic energies of the two spherical pendulums

$$T(q, \dot{q}) = \frac{1}{2}mL^2\|\dot{q}_1\|^2 + \frac{1}{2}mL^2\|\dot{q}_2\|^2. \quad (3.15)$$

The elastic potential energy is assumed to be proportional to $(1 - \cos \theta)$, where θ is the angle between the two pendulum links. Since $\cos \theta = q_1^T q_2$, the elastic potential energy can be expressed in terms of the configuration as

$$U(q) = \kappa(1 - q_1^T q_2), \quad (3.16)$$

where κ is a positive elastic stiffness constant. Note that the elastic potential energy has zero gradient, and hence the force vanishes when the two pendulums are collinear; that is, the angle between the two pendulums is either 0 radians or π radians. The Lagrangian function for the two elastically connected spherical pendulum is thus given by

$$L(q, \dot{q}) = \frac{1}{2}mL^2\|\dot{q}_1\|^2 + \frac{1}{2}mL^2\|\dot{q}_2\|^2 - \kappa(1 - q_1^T q_2). \quad (3.17)$$

The inertia matrix is constant so that the Euler–Lagrange equations, according to Eq. (5.10), are

$$mL^2\ddot{q}_1 + mL^2\|\dot{q}_1\|^2q_1 - \kappa(I_{3 \times 3} - q_1 q_1^T)q_2 = 0, \quad (3.18)$$

$$mL^2\ddot{q}_2 + mL^2\|\dot{q}_2\|^2q_2 - \kappa(I_{3 \times 3} - q_2 q_2^T)q_1 = 0. \quad (3.19)$$

This version of the Euler–Lagrange equations describes the Lagrangian dynamics of the two elastically connected spherical pendulums in terms of $(q, \dot{q}) \in T(S^2)^2$ on the tangent bundle of the configuration manifold $(S^2)^2$.

3.5.2 Euler–Lagrange Equations in Terms of (q, ω)

An alternative version of the Euler–Lagrange equations of motion for the two elastically connected spherical pendulums is expressed in terms of the angular velocity vector of the two links. The rotational kinematics are given by

$$\dot{q}_1 = S(\omega_1)q_1, \quad (3.20)$$

$$\dot{q}_2 = S(\omega_2)q_2, \quad (3.21)$$

where the angular velocity vector $\omega = (\omega_1, \omega_2) \in T_q(S^2)^2$. The modified Lagrangian can be expressed in terms of the angular velocity vector as

$$L^\sim(q, \omega) = \frac{1}{2}mL^2\|\omega_1\|^2 + \frac{1}{2}mL^2\|\omega_2\|^2 - \kappa(1 - q_1^T q_2). \quad (3.22)$$

Following the prior results in Eq. (5.17), the Euler–Lagrange equations for the elastically connected spherical pendulums, expressed in terms of the angular velocity vector, are

$$mL^2\dot{\omega}_1 + \kappa S(q_2)q_1 = 0, \quad (3.23)$$

$$mL^2\dot{\omega}_2 + \kappa S(q_1)q_2 = 0. \quad (3.24)$$

3.6 Filter Design and Initialization

The state of the system is embedded in $SO(3) \times \mathbb{R}^3$ with left multiplication. The propagation noise covariance matrix, measurement noise covariance matrix, and initial uncertainty matrix are appropriately defined. The UKF is initialized with the chosen parameters and state.

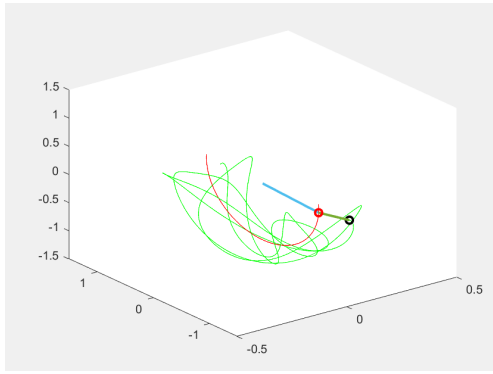


Fig. 3.6: Double Pendulum Simulation.

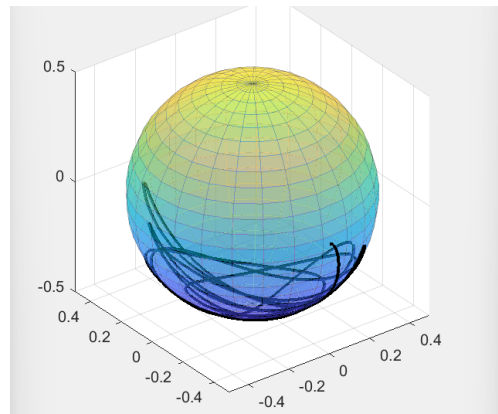


Fig. 3.7: Double Pendulum Trajectory.

3.7 Filtering

The UKF proceeds with a standard Kalman filter loop involving state propagation and update steps based on received measurements. The estimates of the state and covariance are recorded along the trajectory.

3.8 Results

The results showcase the accuracy, robustness, and consistency of the UKF in estimating the position of the spherical pendulum, even in the presence of initial solid errors. Plots depict the pendulum's position as a function of time, along with 3σ interval confidence, demonstrating the convergence to the actual state and the consistency of the filter.

3.9 Conclusion

This chapter demonstrates the successful application of the UKF on parallelizable manifolds for estimating the position of a spherical pendulum. The filter exhibits accuracy, robustness, and consistency, laying the groundwork for further exploration and application in diverse scenarios.

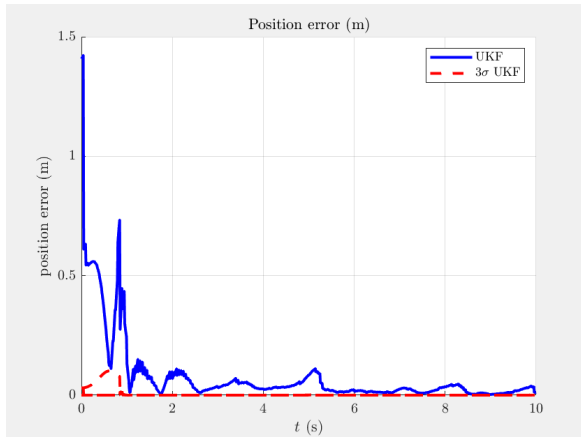


Fig. 3.8: Position Error vs time for UKF and $3 - \sigma$ UKF for Spherical Pendulum.

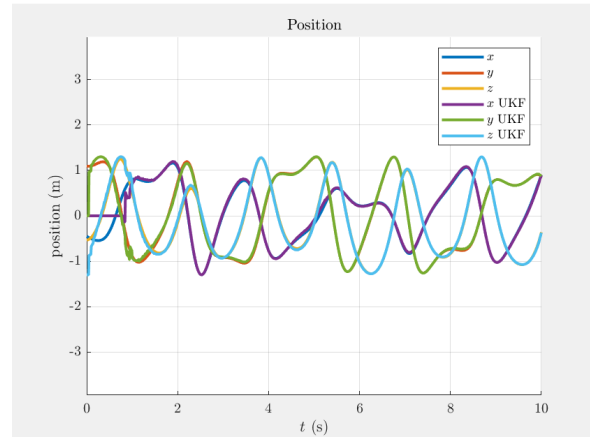


Fig. 3.9: Comparision of True Path and UKF path as Spherical Pendulum evolves with time.

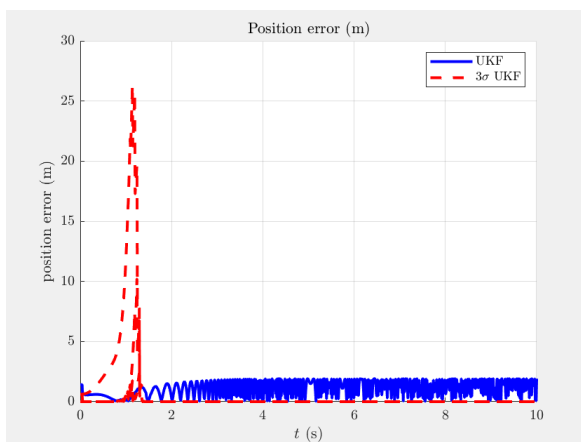


Fig. 3.10: Position Error vs time for UKF and $3 - \sigma$ UKF for Pendulum-Cart System.

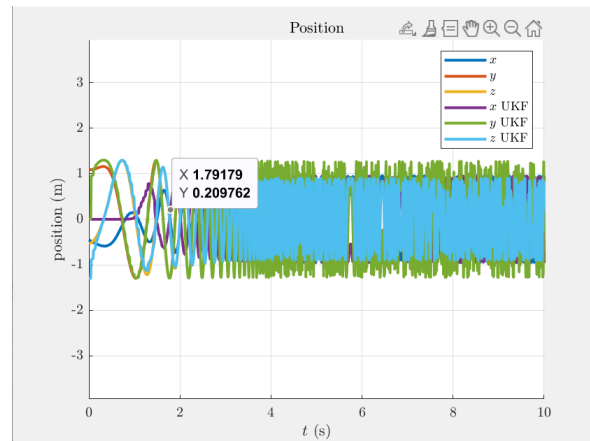


Fig. 3.11: Comparision of True Path and UKF path as Pendulum-Cart evolves with time.

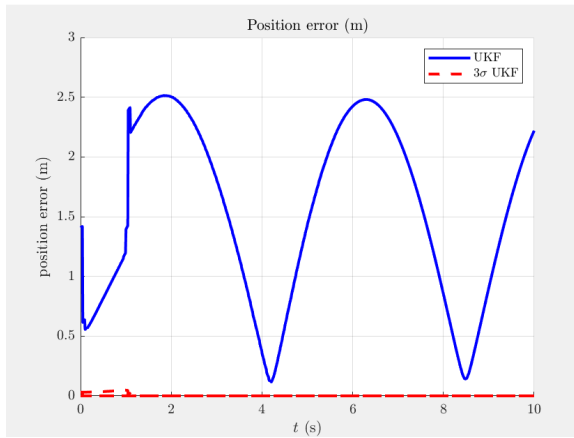


Fig. 3.12: Position Error vs time for UKF and $3 - \sigma$ UKF for Duffing Oscillator.

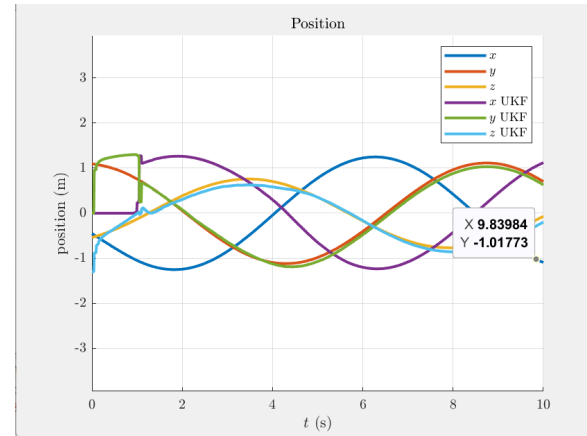


Fig. 3.13: Comparision of True Path and UKF path as Duffing Oscillator evolves with time.



Fig. 3.14: Position Error vs time for UKF and $3 - \sigma$ UKF for Double Pendulum.

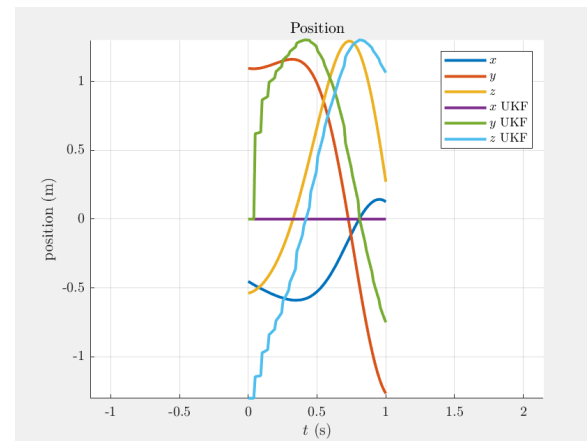


Fig. 3.15: Comparision of True Path and UKF path as Double Pendulum evolves with time.

Chapter 4

Case Study

The Filter Accuracy of the dynamic and measurement models directly influences the filter's ability to estimate the true state. The filter may provide inaccurate estimates if the models poorly represent the system dynamics or measurements.

The parameters which can be tuned to make the filer better are:

- Initial Conditions and Uncertainty
- Noise Level
- Sigma Point Parameters
- Covariation Matrix
- Integration step size
- Number of Epochs
- Filter Parameters

Now, we will discuss how changing the filter can be designed better by adjusting these factors.

4.1 Duffing Oscillator

4.1.1 Base Case

Here the length of the pendulum is 1.3m

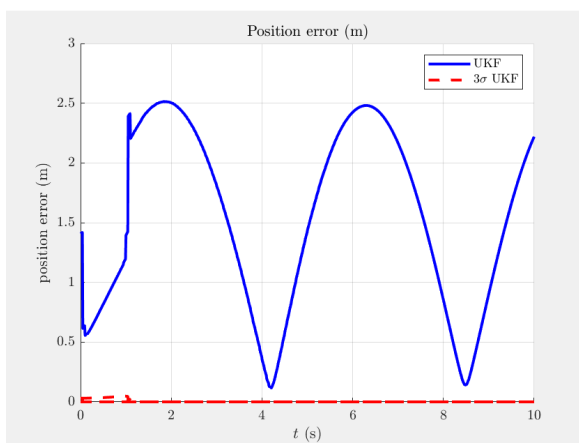


Fig. 4.1: Position Error vs time for UKF and $3-\sigma$ UKF for Duffing Oscillator in base case

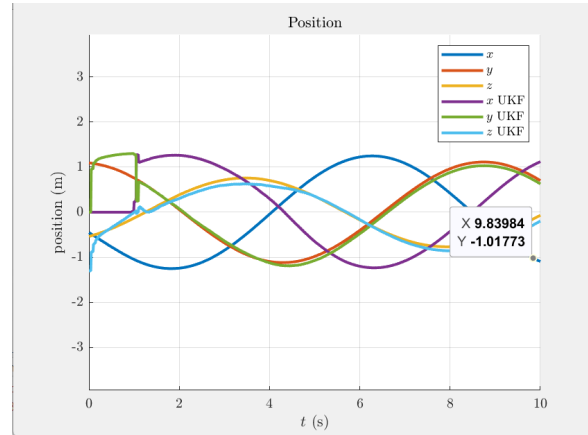


Fig. 4.2: Position of the components of Duffing Oscillator as a function of time. and Estimated position from the Unscented Kalman Filter (UKF) in base case

4.1.2 Plots in XY, YZ and ZX Plane

Base case is as follows

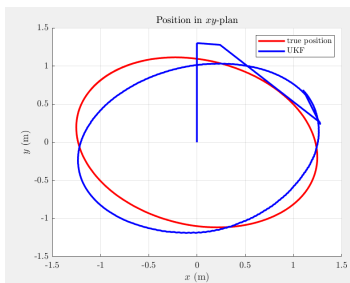


Fig. 4.3: True vs Es-
timated Position (Basetted Position) in XY plane

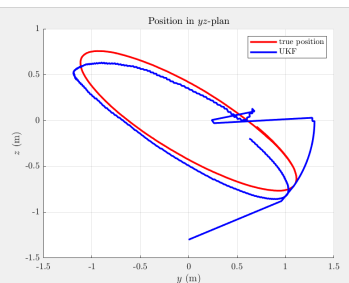


Fig. 4.4: True vs Es-
timated Position (Basetted Position) in YZ plane

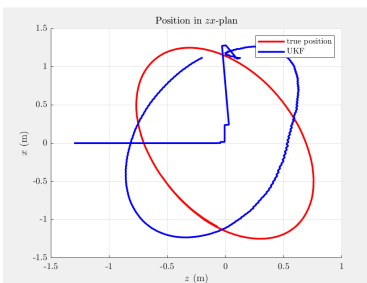


Fig. 4.5: True vs Es-
timated Position (Basetted Position) in ZX plane

4.1.3 High Noise

The new noise matrix is

$$C = \begin{pmatrix} \frac{1}{180\pi} \\ \frac{1}{180\pi} \end{pmatrix} \quad (4.1)$$

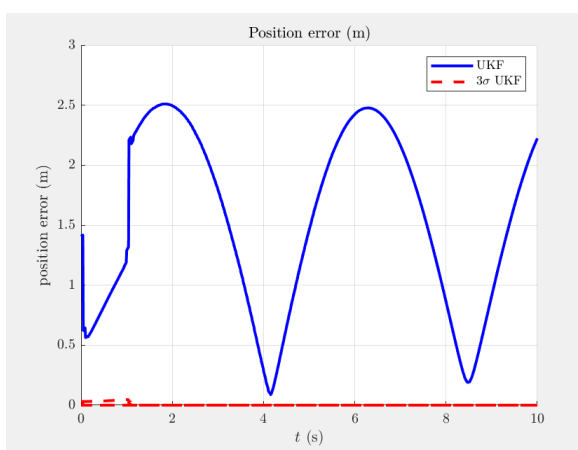


Fig. 4.6: Position Error vs time for UKF and $3-\sigma$ UKF for Duffing Oscillator in high noise case

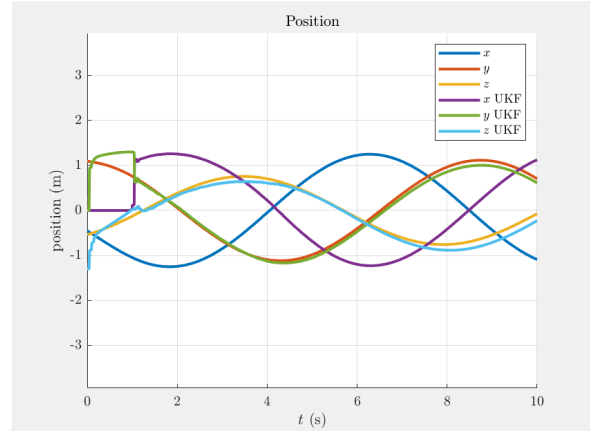


Fig. 4.7: Position of the components of Duffing Oscillator as a function of time and Estimated position from the Unscented Kalman Filter (UKF) in high noise case

4.1.4 Plots in XY, YZ and ZX Plane

High noise case is as follows

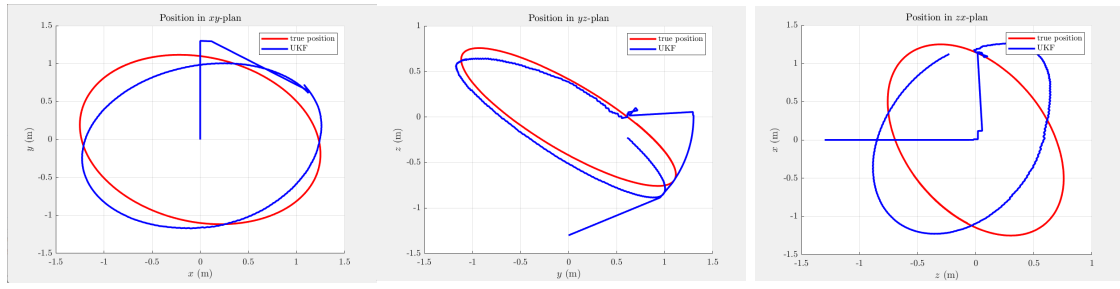


Fig. 4.8: True vs Estimated Position (High Noise Case) in XY plane

Fig. 4.9: True vs Estimated Position (High Noise Case) in YZ plane

Fig. 4.10: True vs Estimated Position (High Noise Case) in ZX plane

4.1.5 Increased Number of Epochs

Here We increased the epochs to fine grain the integration process.

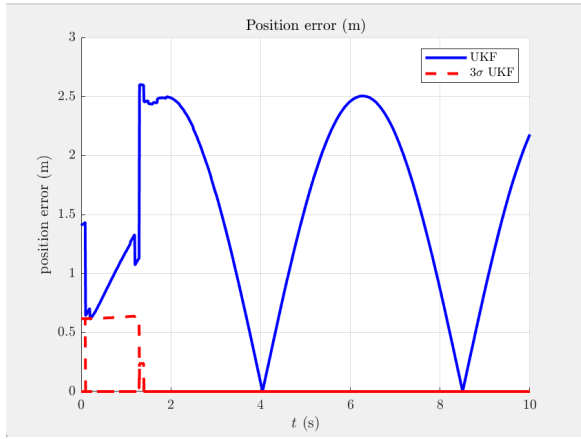


Fig. 4.11: Position Error vs time for UKF and $3 - \sigma$ UKF for Duffing Oscillator with increased number of epochs

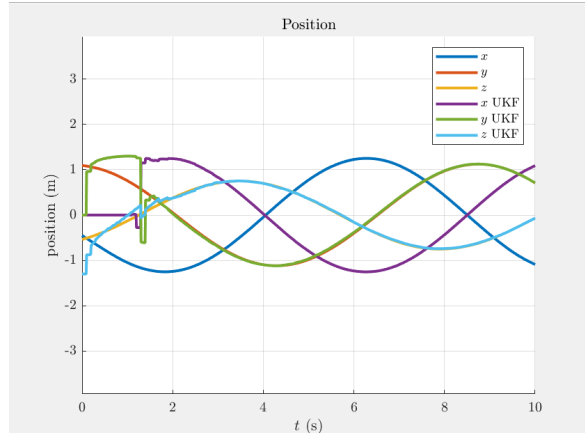


Fig. 4.12: Position of the components of Duffing Oscillator as a function of time and Estimated position from the Unscented Kalman Filter (UKF) with increased number of epochs

4.1.6 Plots in XY, YZ and ZX Plane

The increased number of epochs case is as follows

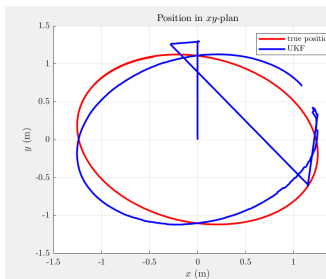


Fig. 4.13: True vs Estimated Position (Increased Number of Epochs Case) in XY plane

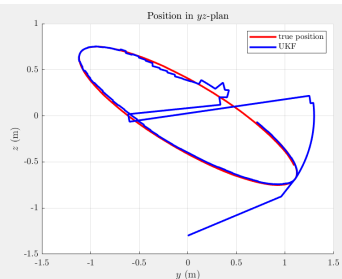


Fig. 4.14: True vs Estimated Position (Increased Number of Epochs Case) in YZ plane

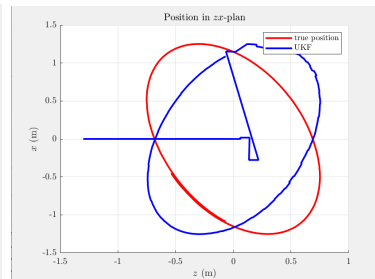


Fig. 4.15: True vs Estimated Position (Increased Number of Epochs Case) in ZX plane

4.1.7 Uncertainty Matrix

Here the new uncertainty matrix is

$$P_0 = \begin{bmatrix} \left(\frac{10}{180\pi}\right)^2 & 0 & 0 \\ 0 & \left(\frac{10}{180\pi}\right)^2 & 0 \\ 0 & 0 & \left(\frac{10}{180\pi}\right)^2 \end{bmatrix} \quad (4.2)$$

The initial uncertainty matrix was

$$P_0 = \begin{bmatrix} \left(\frac{45}{180\pi}\right)^2 & 0 & 0 \\ 0 & \left(\frac{45}{180\pi}\right)^2 & 0 \\ 0 & 0 & \left(\frac{45}{180\pi}\right)^2 \end{bmatrix} \quad (4.3)$$

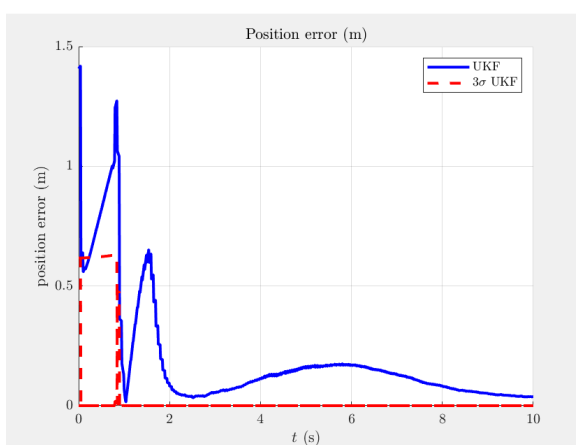


Fig. 4.16: Position Error vs time for UKF and $3 - \sigma$ UKF for Duffing Oscillator with uncertainty matrix

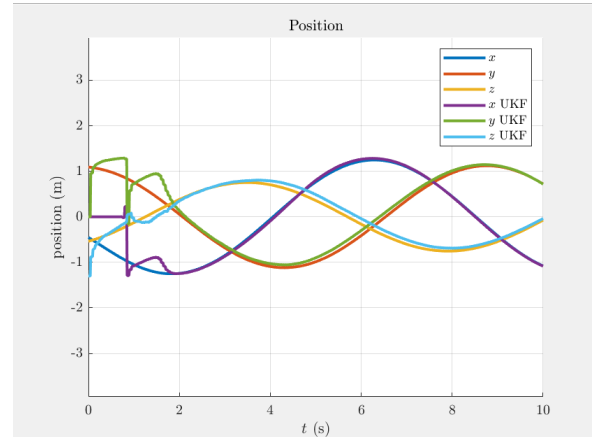


Fig. 4.17: Position of the components of Duffing Oscillator as a function of time and Estimated position from the Unscented Kalman Filter (UKF) with uncertainty matrix

4.1.8 Plots in XY, YZ and ZX Plane

The uncertainty matrix case is as follows

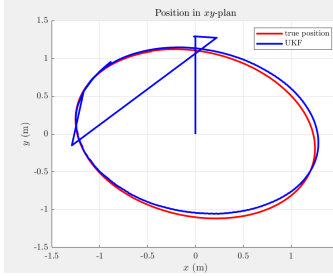


Fig. 4.18: True vs Estimated Position (Uncertainty Matrix Case) in XY plane

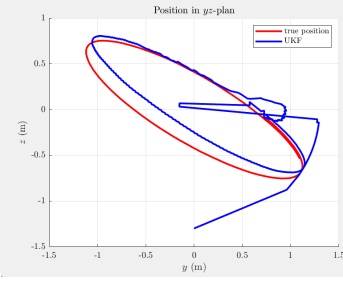


Fig. 4.19: True vs Estimated Position (Uncertainty Matrix Case) in YZ plane

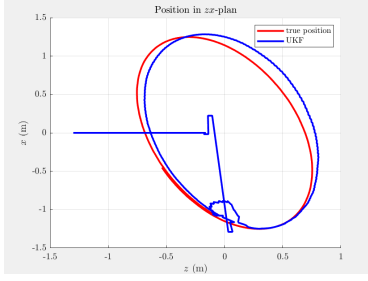


Fig. 4.20: True vs Estimated Position (Uncertainty Matrix Case) in ZX plane

4.2 Spherical Pendulum

4.2.1 Base Case

Here, we consider the base case scenario.

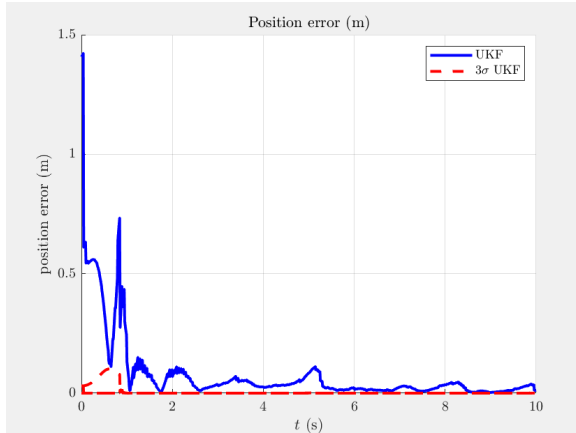


Fig. 4.21: Position Error vs time for UKF and $3 - \sigma$ UKF for Spherical Pendulum in the base case

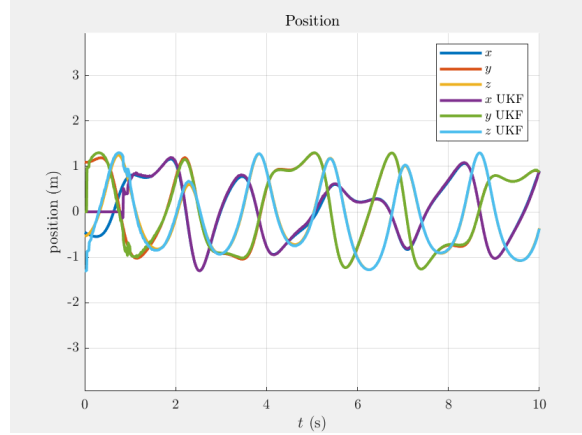


Fig. 4.22: Position of the components of Spherical Pendulum as a function of time and Estimated position from the Unscented Kalman Filter (UKF) in the base case

4.2.2 Plots in XY, YZ and ZX Plane

The base case is as follows

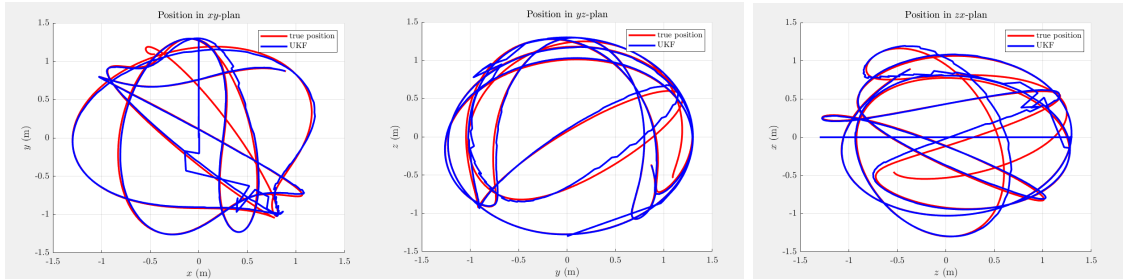


Fig. 4.23: True vs Estimated Position (Base Case) in XY plane

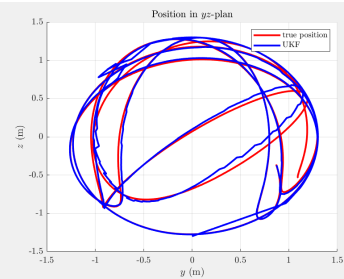


Fig. 4.24: True vs Estimated Position (Base Case) in YZ plane

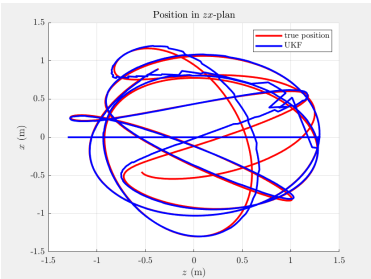


Fig. 4.25: True vs Estimated Position (Base Case) in ZX plane

4.2.3 High Noise Std Deviation

Here, the noise level is increased for the simulation.

$$C = \begin{pmatrix} \frac{1}{18\pi} \\ \frac{1}{18\pi} \end{pmatrix}$$

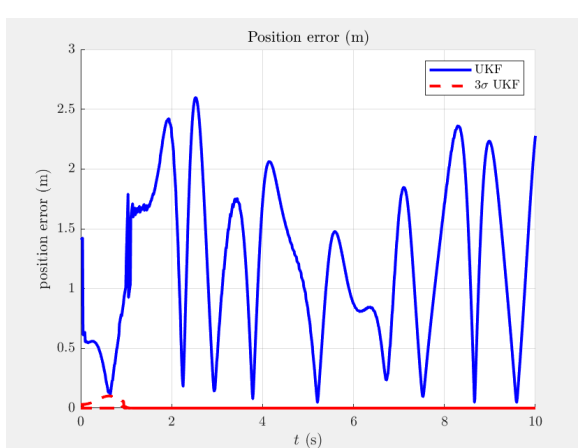


Fig. 4.26: Position Error vs time for UKF and $3-\sigma$ UKF for Spherical Pendulum with high noise

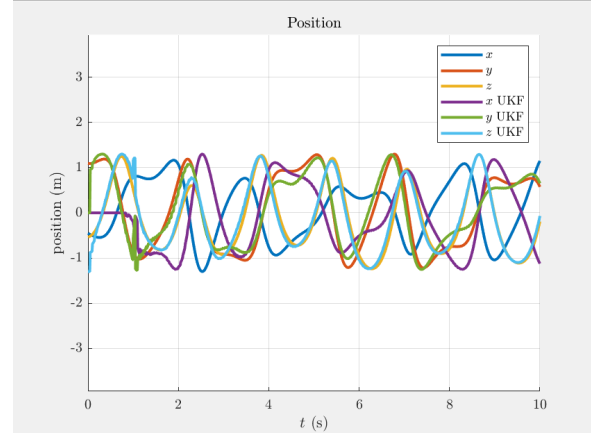


Fig. 4.27: Position of the components of Spherical Pendulum as a function of time and Estimated position from the Unscented Kalman Filter (UKF) with high noise

4.2.4 Plots in XY, YZ and ZX Plane

The high noise case is as follows

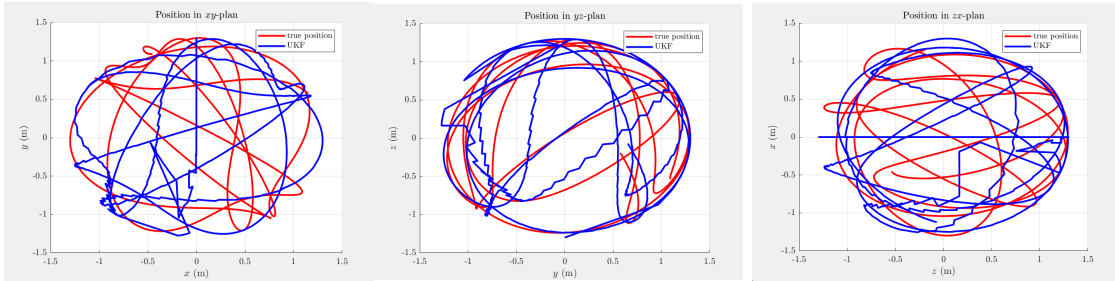


Fig. 4.28: True vs Estimated Position (High Noise Case) in XY plane

Fig. 4.29: True vs Estimated Position (High Noise Case) in YZ plane

Fig. 4.30: True vs Estimated Position (High Noise Case) in ZX plane

4.2.5 Low Noise Std Deviation

Here, the noise level for the simulation is decreased.

$$C = \begin{pmatrix} \frac{1}{360\pi} \\ \frac{1}{360\pi} \end{pmatrix}$$

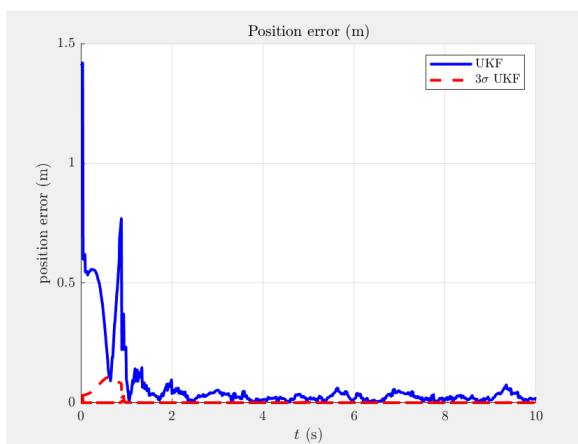


Fig. 4.31: Position Error vs time for UKF and $3-\sigma$ UKF for Spherical Pendulum with low noise

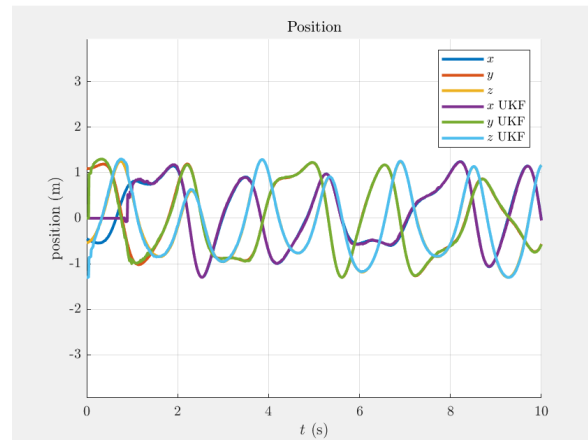


Fig. 4.32: Position of the components of Spherical Pendulum as a function of time and Estimated position from the Unscented Kalman Filter (UKF) with low noise

4.2.6 Plots in XY, YZ and ZX Plane

The low noise case is as follows

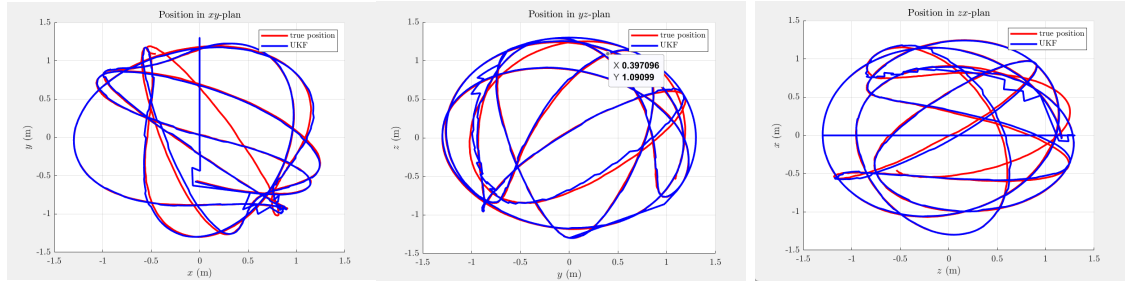


Fig. 4.33: True vs Estimated Position (Low Noise Case) in XY plane

Fig. 4.34: True vs Estimated Position (Low Noise Case) in YZ plane

Fig. 4.35: True vs Estimated Position (Low Noise Case) in ZX plane

4.2.7 Change in Initial Condition ($l = 5$)

Here, we consider a scenario where the initial length condition l is set to 5.

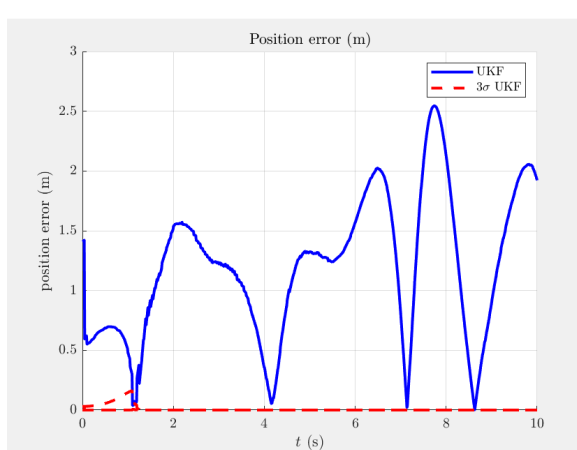


Fig. 4.36: Position Error vs time for UKF and 3σ UKF for Spherical Pendulum with $l = 5$

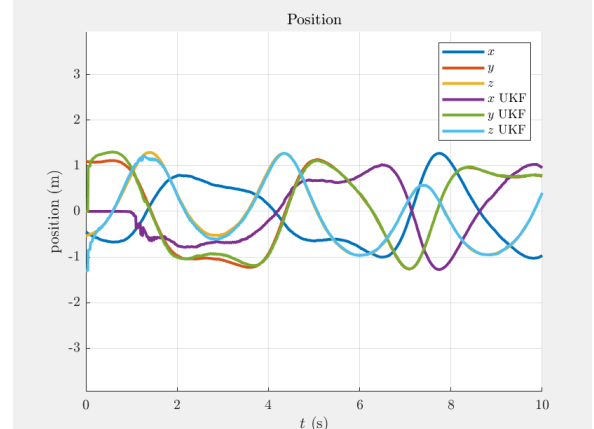


Fig. 4.37: Position of the components of Spherical Pendulum as a function of time and Estimated position from the Unscented Kalman Filter (UKF) with $l = 5$

4.2.8 Plots in XY, YZ and ZX Plane

The case with $l = 5$ is as follows

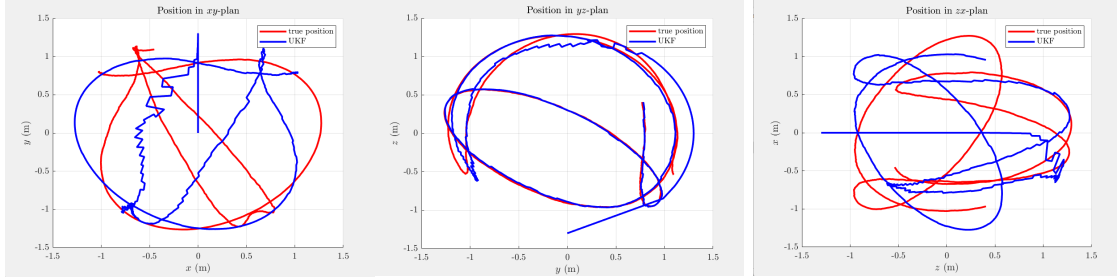


Fig. 4.38: True vs Estimated Position ($l = 5$) in XY plane

Fig. 4.39: True vs Estimated Position ($l = 5$) in YZ plane

Fig. 4.40: True vs Estimated Position ($l = 5$) in ZX plane

4.3 Double Pendulum

Here, we consider the base case scenario.

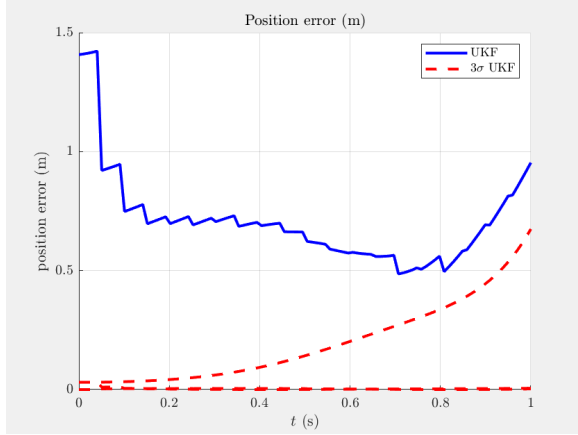


Fig. 4.41: Position Error vs time for UKF and $3 - \sigma$ UKF for Spherical Pendulum in the base case

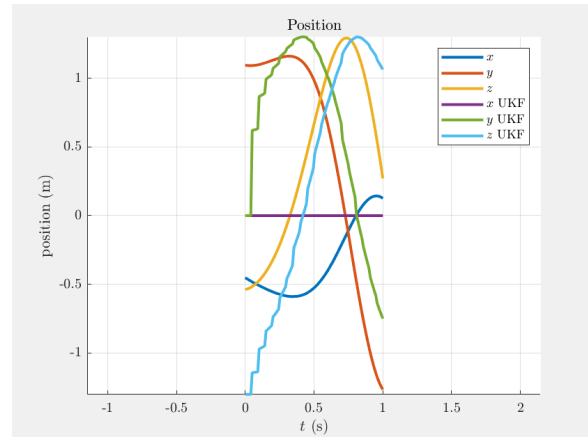


Fig. 4.42: Position of the components of Spherical Pendulum as a function of time and Estimated position from the Unscented Kalman Filter (UKF) in the base case

4.3.1 Plots in XY, YZ and ZX Plane

The base case is as follows

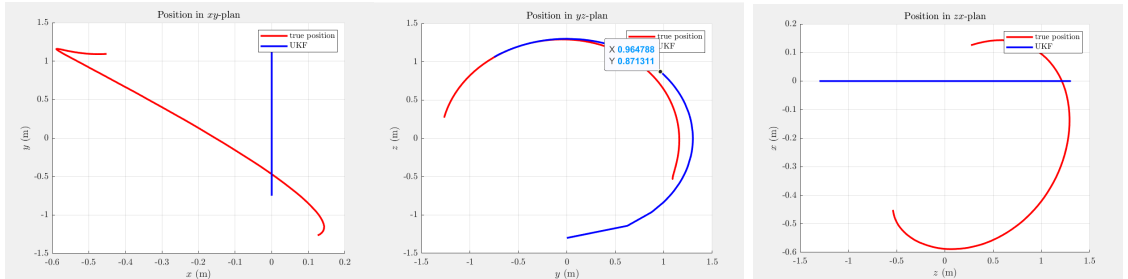


Fig. 4.43: True vs Estimated Position (Base Case) in XY plane

Fig. 4.44: True vs Estimated Position (Base Case) in YZ plane

Fig. 4.45: True vs Estimated Position (Base Case) in ZX plane

4.4 Pendulum Cart

Here, we consider the base case scenario.

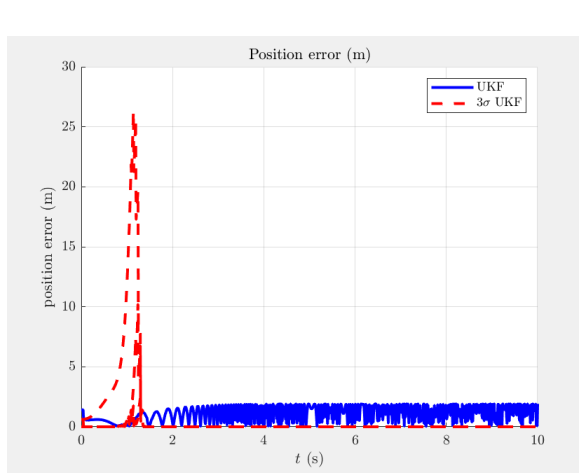


Fig. 4.46: Position Error vs time for UKF and $3 - \sigma$ UKF for Spherical Pendulum in the base case

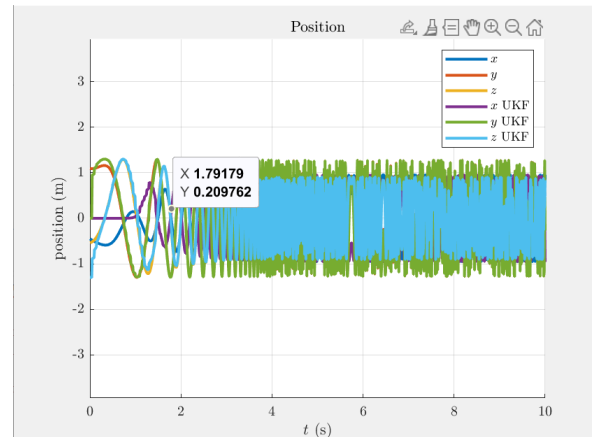


Fig. 4.47: Position of the components of Spherical Pendulum as a function of time and Estimated position from the Unscented Kalman Filter (UKF) in the base case

4.4.1 Plots in XY, YZ and ZX Plane

The base case is as follows

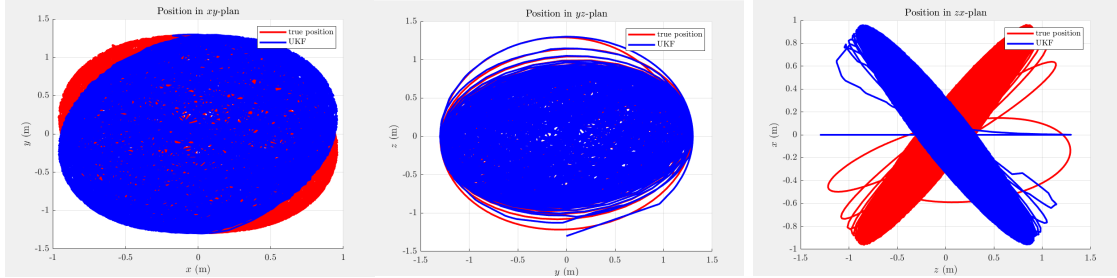


Fig. 4.48: True vs Estimated Position (Base Case) in XY plane **Fig. 4.49:** True vs Estimated Position (Base Case) in YZ plane **Fig. 4.50:** True vs Estimated Position (Base Case) in ZX plane

In this case study, we explored how different conditions affect the filter. Here, we explored one case for each system, i.e., the Spherical Pendulum and Duffing oscillator, and the results were similar for the other two dynamical systems.

Chapter 5

Conclusion and Future Work

The exploration of state and parameter estimation on manifolds using Lie groups has opened up exciting avenues for future research and practical applications, especially in the realms of structural engineering and control. This chapter outlines potential future directions and use cases, pointing towards this innovative approach's continued evolution and application.

5.1 Development of UKF-M

Currently, we focussed completely on simulating the system and then used Lie groups and Lie algebra to ease up our work, however, to develop more accurate filters there is a lot of scope for research on Improving the methods estimate state and parameters using Kalman Filter directly using the properties of manifolds and generalizing it to all manifolds.

5.2 Advanced State Estimation Techniques

Future research endeavors can delve into developing advanced state estimation techniques, further harnessing the capabilities of the Lie group framework. This entails refining algorithms and methodologies for precisely estimating dynamic system states on manifolds

such as the Special Orthogonal Group $SO(3)$ or other Lie groups. Improved accuracy and robustness in state estimation can empower more effective control strategies for intricate systems.

5.3 Parameter Estimation on Manifolds

Extending state estimation to parameter estimation is a promising avenue for future exploration. Structural systems often feature parameters with variability or uncertainty, such as mass distributions, material properties, and damping coefficients. Future research can focus on developing methods that concurrently estimate the system state and its parameters, considering the inherent manifold structure. This holistic approach enhances our ability to model and control complex systems effectively.

5.4 De-tuning Strategies

A practical application of state and parameter estimation on manifolds lies in detuning – adjusting system parameters, such as damping properties of tuned mass dampers, to optimize structural performance. Subsequent research can investigate how Lie group-based estimation techniques contribute to adaptively retuning systems, enabling them to counteract changing environmental conditions and ensuring structural stability and safety.

5.5 Adaptive Tuning of TMDs and Developments of Active and Passive Controllers on manifolds

Adaptive tuning involves dynamically adjusting the parameters of a structure or its control systems in response to varying loads or external factors. Lie group-based estimation is poised to play a pivotal role in developing adaptive tuning strategies for structures equipped with tuned mass dampers. These strategies can optimize damper performance in real time,

reducing structural vibrations and enhancing overall system efficiency.

5.6 Health Monitoring and Maintenance

State and parameter estimation techniques on manifolds find applications in health monitoring and maintenance of structures. Continuous monitoring of a structure's state and parameters, including those of tuned mass dampers, facilitates the detection of anomalies and degradation. This proactive approach to maintenance can significantly extend the lifespan of structures, bolstering safety and structural integrity.

5.7 Conclusion

As we embark on these future research directions and applications, integrating Lie groups into state and parameter estimation methodologies promises to revolutionize our structural engineering and control approach. These endeavors can potentially create more resilient, adaptive, and efficient systems across various domains.

Chapter 6

Appendix

6.1 Software Used

During Phase 1 of this work, preliminary studies were conducted using Python 3.10. However, for the subsequent programming and simulation tasks, MATLAB was chosen as the preferred tool. MATLAB offers powerful computational capabilities, with an easy-to-understand syntax and a comprehensive set of built-in linear algebra functions, which greatly simplifies the programming process. Notably, the presence of MATLAB's symbolic toolbox was particularly advantageous, as it facilitated the implementation of complex formulations, such as the Kolmogorov Operators, and the Estimation of Sigma Points. While Python has libraries like SymPy for symbolic computations, it is not as robust and integrated as MATLAB's symbolic toolbox. Thus, MATLAB was chosen for this phase of the work to leverage its strengths in symbolic calculations.

The plots presented in this work were entirely generated using MATLAB's built-in functions, which provided efficient and visually appealing representations of the data.

6.2 Appendix

Given the extensive nature of the numerical computations and the code base developed for this thesis work, we have provided a GitHub Repository link for easy access. This link allows users to access the code repository at any time, allowing them to explore and utilize the code as needed. Link: <https://github.com/Roshan818/State-and-Parameter-Estimation.git>

References

- [1] A. Roffel and S. Narasimhan, “Extended kalman filter for modal identification of structures equipped with a pendulum tuned mass damper,” *Journal of Sound and Vibration*, vol. 333, no. 23, pp. 6038–6056, 2014.
- [2] S. Hauberg, F. Lauze, and K. S. Pedersen, “Unscented kalman filtering on riemannian manifolds,” *Journal of mathematical imaging and vision*, vol. 46, pp. 103–120, 2013.
- [3] S. Panda, T. Tripura, and B. Hazra, “First-order error-adapted eigen perturbation for real-time modal identification of vibrating structures,” *Journal of Vibration and Acoustics*, vol. 143, no. 5, p. 051001, 2021.
- [4] X. Pennec, “Intrinsic statistics on riemannian manifolds: Basic tools for geometric measurements,” *Journal of Mathematical Imaging and Vision*, vol. 25, pp. 127–154, 2006.
- [5] S. Panda and B. Hazra, “Stochastic dynamics on manifolds based on novel geometry preserving ito–taylor scheme,” *Journal of Sound and Vibration*, vol. 550, p. 117599, 2023.
- [6] S. Särkkä and A. Solin, *Applied stochastic differential equations*, vol. 10. Cambridge University Press, 2019.

- [7] R. Prasad, S. Panda, and B. Hazra, “A new symplectic integrator for stochastic hamiltonian systems on manifolds,” *Probabilistic Engineering Mechanics*, vol. 74, p. 103526, 2023.
- [8] V. G. Ivancevic and T. T. Ivancevic, “Lecture notes in lie groups,” 2011.
- [9] A. Pressley, *Elementary Differential Geometry*. Springer Undergraduate Mathematics Series, Springer London, 2010.
- [10] J. Sola, J. Deray, and D. Atchuthan, “A micro lie theory for state estimation in robotics,” *arXiv preprint arXiv:1812.01537*, 2018.
- [11] E. Y. Gu, *Advanced Dynamics Modeling, Duality and Control of Robotic Systems*. CRC Press, 2021.
- [12] D. Simon, “Kalman filtering,” *Embedded systems programming*, vol. 14, no. 6, pp. 72–79, 2001.
- [13] E. A. Wan and R. Van Der Merwe, “The unscented kalman filter for nonlinear estimation,” in *Proceedings of the IEEE 2000 adaptive systems for signal processing, communications, and control symposium (Cat. No. 00EX373)*, pp. 153–158, Ieee, 2000.
- [14] M. Brossard, A. Barrau, and S. Bonnabel, “A Code for Unscented Kalman Filtering on Manifolds (UKF-M),” 2019.
- [15] J. L. Crassidis, “Sigma-point kalman filtering for integrated gps and inertial navigation,” *IEEE Transactions on Aerospace and Electronic Systems*, vol. 42, no. 2, pp. 750–756, 2006.
- [16] H. M. Menegaz, J. Y. Ishihara, and H. T. Kussaba, “Unscented kalman filters for riemannian state-space systems,” *IEEE Transactions on Automatic Control*, vol. 64, no. 4, pp. 1487–1502, 2018.

- [17] H. M. T. Menegaz, “Unscented kalman filtering on euclidean and riemannian manifolds,” 2016.
- [18] T. Lee, M. Leok, and N. H. McClamroch, “Global formulations of lagrangian and hamiltonian dynamics on manifolds,” *Springer*, vol. 13, p. 31, 2017.
- [19] S. Panda, A. Gogoi, B. Hazra, and V. Pakrashi, “Geometry preserving ito-taylor formulation for stochastic hamiltonian dynamics on manifolds,” *Applied Mathematical Modelling*, vol. 119, pp. 626–647, 2023.
- [20] I. Kovacic and M. J. Brennan, *The Duffing equation: nonlinear oscillators and their behaviour*. John Wiley & Sons, 2011.
- [21] S. Fiori, I. Cervigni, M. Ippoliti, and C. Menotta, “Synthetic nonlinear second-order oscillators on riemannian manifolds and their numerical simulation,” *Discrete and Continuous Dynamical Systems-B*, vol. 27, no. 3, pp. 1227–1262, 2022.